Dishevelled stabilization by the ciliopathy protein Rpgrip1l is essential for planar cell polarity

Alexia Mahuzier,[1,2] Helori-Mael Gaudé,[3,4] Valentina Grampa,[3,4] Isabelle Anselme,[1,2] Flora Silbermann,[3,4] Margot Leroux-Berger,[1,2] Delphine Delacour,[5] Jerome Ezan,[6] Mireille Montcouquiol,[6] Sophie Saunier,[3,4] Sylvie Schneider-Maunoury,[1,2] and Christine Vesque[1,2]

[1]Centre National de la Recherche Scientifique (CNRS) UMR 7622, Institut National de la Santé et de la Recherche Médicale (INSERM) U969, 75005 Paris, France
[2]Université Pierre et Marie Curie, 75005 Paris, France
[3]INSERM, U983, Hôpital Necker-Enfants Malades, 75015 Paris, France
[4]Université Paris-Descartes, Sorbonne Paris Cité, Faculté de Médecine, 75015 Paris, France
[5]Institut Jacques-Monod, CNRS-UMR7592, Université Paris 7, 75013 Paris, France
[6]INSERM U862, Université Bordeaux 2, 33077 Bordeaux, France

Cilia are at the core of planar polarity cellular events in many systems. However, the molecular mechanisms by which they influence the polarization process are unclear. Here, we identify the function of the ciliopathy protein Rpgrip1l in planar polarity. In the mouse cochlea and in the zebrafish floor plate, Rpgrip1l was required for positioning the basal body along the planar polarity axis. Rpgrip1l was also essential for stabilizing dishevelled at the cilium base in the zebrafish floor plate and in mammalian renal cells. In rescue experiments, we showed that in the zebrafish floor plate the function of Rpgrip1l in planar polarity was mediated by dishevelled stabilization. In cultured cells, Rpgrip1l participated in a complex with inversin and nephrocystin-4, two ciliopathy proteins known to target dishevelled to the proteasome, and, in this complex, Rpgrip1l prevented dishevelled degradation. We thus uncover a ciliopathy protein complex that finely tunes dishevelled levels, thereby modulating planar cell polarity processes.

Introduction

Many epithelia are characterized by a coordinated polarization of cells along the plane of the tissue, called planar cell polarity (PCP). This property has been extensively studied in *Drosophila*, where many actors involved in this process have been identified. Central to this process is the "core" PCP pathway, which involves the transmembrane proteins Frizzled (Fz), Strabismus/Van Gogh (Stbm/Vang), and Flamingo (Fmi), as well as the cytosolic proteins Dishevelled (Dsh), Diego (Dgo), and Prickle (Pk). These proteins are enriched at adherens junctions and form two asymmetric complexes, localized at opposite positions along the planar polarity axis of the cell (Goodrich and Strutt, 2011). In vertebrates, one of the best model systems to study PCP is found in the mammalian cochlea, where all the mechanosensory cells in the organ of Corti possess a V- or W-shaped, actin-based stereociliary bundle with stereotyped orientation along the plane of the epithelium (Jones and Chen, 2008). Other examples of PCP signaling-dependent mechanisms in vertebrates include polarized cell intercalation and directed cell migration leading to convergence-extension (CE) movements (Karner et al., 2009; Roszko et al., 2009), and oriented cell division (Fischer and Pontoglio, 2009; Ségalen et al., 2010), which occur during gastrulation, neurulation, and renal tubule elongation. Proteins involved in vertebrate PCP, including the Stbm/Vang orthologue Van Gogh-like (Vangl2), Frizzled (Fz3/6), Prickle (Pk1/2), and Dishevelled (Dvl1-3), are distributed asymmetrically in the mouse cochlear and vestibular hair cells (Wang et al., 2005; Montcouquiol et al., 2006; Deans et al., 2007; Narimatsu et al., 2009).

Cilia are microtubule-based organelles projecting out from the cell surface of most eukaryotic cells and performing motile and/or sensory functions. In vertebrates, primary (nonmotile) cilia are present in virtually all cells and are involved in the Hedgehog (Hh), PDGFa, Notch, and Wnt pathways (Goetz and

A. Mahuzier and H.-M. Gaudé contributed equally to this paper.

Correspondence to Sylvie Schneider-Maunoury: sylvie.schneider-maunoury@snv.jussieu.fr; or Christine Vesque: christine.vesque@snv.jussieu.fr.

Abbreviations used in this paper: βgal, β-galactosidase; CE, convergence-extension; Dsh, Dishevelled; hpf, hours post-fertilization; PCP, planar cell polarity.

The Rockefeller University Press $30.00
J. Cell Biol. Vol. 198 No. 5 927–940
www.jcb.org/cgi/doi/10.1083/jcb.201111009

Anderson, 2010; Ezratty et al., 2011). Cilium dysfunctions have been causally linked to a group of pleiotropic and genetically heterogeneous human diseases, the so-called ciliopathies (Badano et al., 2006; Sharma et al., 2008; Cardenas-Rodriguez and Badano, 2009). Ciliogenesis and cilium function rely on intraflagellar transport (IFT), a polarized, bidirectional transport system involving IFT protein complexes and molecular motors tracking along the ciliary axoneme. In addition, the ciliopathy proteins BBS, MKS, and NPHP, involved in Bardet-Biedl syndromes, Meckel syndromes, and nephronophthisis, respectively, form different protein complexes at the base of the cilium and participate in its assembly and function. MKS and NPHP proteins contribute to establish the ciliary gate that controls the entry and exit of ciliary proteins (Dowdle et al., 2011; Garcia-Gonzalo et al., 2011; Williams et al., 2011; Zhao and Malicki, 2011).

Recent studies have revealed roles for ciliary proteins in planar polarity establishment in different experimental models. Zebrafish embryos depleted in Bbs proteins show CE defects enhanced by reduction in core PCP protein amounts (Ross et al., 2005; Gerdes et al., 2007; May-Simera et al., 2009). Moreover, mouse *Ift88* and *Bbs* mutants show planar polarity defects in the cochlea (Ross et al., 2005; Jones et al., 2008). In several instances, the cilium itself acquires a polarized position within the cell and/or a polarized orientation of its basal body, and thereby constitutes a readout of planar polarity (Wallingford, 2010). This is the case for the multicilia of the *Xenopus* larval skin (Park et al., 2008; Mitchell et al., 2009) and of mammalian ependymal cells (Guirao et al., 2010), as well as for monocilia in the mouse node (Song et al., 2010), in the cochlea (Jones and Chen, 2008), and in the zebrafish floor plate (Borovina et al., 2010). This planar polarization of the cilium requires the core PCP genes *Vangl1/2*, *Fz*, and *Dvl* (Montcouquiol et al., 2003; Park et al., 2008; Borovina et al., 2010; Hashimoto et al., 2010; Song et al., 2010).

The level at which cilia are involved in planar polarity, and their link with PCP signaling, are unclear. In the mouse cochlea, polarity defects are observed in *Ift88* mouse mutants, which show total cilium loss, without disruption of the polarized distribution of the core proteins Vangl2 and Fz3 (Jones et al., 2008). This suggests that cilia act downstream or parallel to the PCP signaling pathway. Other data suggest that cilia mediate a switch between the Wnt–β-catenin and the Wnt-PCP pathways. The basal body protein inversin, the product of the *Nphp2/inversin (inv)* gene, targets cytoplasmic dishevelled for proteasomal degradation (Simons et al., 2005). Inversin negatively regulates Wnt–β-catenin signaling in cultured mammalian cells and in *Xenopus* and zebrafish embryos; conversely, it interacts functionally with the PCP pathway during CE (Simons et al., 2005). Ciliary proteins also negatively control β-catenin stability (Gerdes et al., 2007; Corbit et al., 2008) and nuclear translocation (Lancaster et al., 2011). Several Wnt pathway proteins such as Vangl2, Diversin, β-catenin, and Jouberin, are enriched at the basal body and/or cilium (Ross et al., 2005; Itoh et al., 2009; Guirao et al., 2010; Lancaster et al., 2011), underlining the role of this structure as a regulatory platform for Wnt signaling. Despite these numerous studies, the function of cilia in the Wnt pathways remains poorly understood and controversial (Huang and Schier, 2009; Wallingford and Mitchell, 2011).

To better understand the role of different ciliary protein complexes in vertebrate PCP, we investigated the function of the ciliopathy gene *Rpgrip1l* (also called *Mks5*, *Nphp8,* and, for the mouse gene, *Ftm*) in this process. Rpgrip1l is a 175-kD protein containing several protein–protein interaction domains: three N-terminal coiled-coil domains, two C2 domains, and a C-terminal RPGR-interacting domain (RID; Vierkotten et al., 2007). The protein is mainly found at the ciliary transition zone where it forms a complex with nephrocystin-1 and nephrocystin-4 (*Nphp4* gene; Roepman et al., 2005; Delous et al., 2007; Sang et al., 2011). In *Caenorhabditis elegans* sensory neurons, Rpgrip1l interacts functionally with NPHP and MKS proteins for the formation and function of the ciliary gate (Williams et al., 2011). The human *RPGRIP1L* gene is one of the causal genes in Meckel and Joubert type B syndromes, two autosomal-recessive multisystem ciliopathies characterized by polydactyly, kidney cysts, and central nervous system malformations such as cerebellar vermis hypoplasia and encephalocele (Arts et al., 2007; Delous et al., 2007), and acts as a modifier gene in most ciliopathies (Khanna et al., 2009; Zaghloul and Katsanis, 2010). In mouse, *Rpgrip1l* is required for normal ciliogenesis in some but not all cell types (Arts et al., 2007; Delous et al., 2007; Vierkotten et al., 2007; Besse et al., 2011). Mice with a targeted inactivation of the *Ftm*/*Rpgrip1l* gene die around birth and recapitulate most malformations observed in MKS fetuses, including exencephaly, olfactory bulb agenesis, polydactyly, and kidney cysts (Delous et al., 2007; Vierkotten et al., 2007; Besse et al., 2011). Rpgrip1l is required for the correct regulation of Hh transduction (Vierkotten et al., 2007), and our recent data demonstrate that its function in telencephalic morphogenesis is mediated by the regulation of Gli3 proteolytic processing (Besse et al., 2011). Besides this essential role in Hh/Gli regulation, Rpgrip1l knock-down in zebrafish leads to CE defects, a process that has been linked to PCP signaling (Khanna et al., 2009).

Here, we used different model systems to investigate the function of *Rpgrip1l* in planar polarity and its interaction with the PCP pathway. We showed that *Rpgrip1l* is required for planar polarity in sensory hair cells of the mouse cochlea, in CE during zebrafish gastrulation and neurulation, and in the polarized positioning of motile cilia of the zebrafish floor plate. In the zebrafish floor plate and in cultured mammalian kidney cells, we showed that the enrichment of dishevelled at the base of the cilium was dependent on Rpgrip1l. Rpgrip1l positively controls dishevelled levels, and Dvl overexpression in zebrafish embryos rescues CE and floor plate cilia localization in *rpgrip1l* morphants. We provide a model for Rpgrip1l function in a ciliopathy protein complex modulating dishevelled stability.

Results

Rpgrip1l is essential for localization of the cilium along the PCP axis in cochlear hair cells

Rpgrip1l is present at the kinocilium transition zone in E18.5 cochlear hair cells (Fig. 1 A). To investigate the involvement of Rpgrip1l in PCP, we first analyzed the polarity of cochlear hair

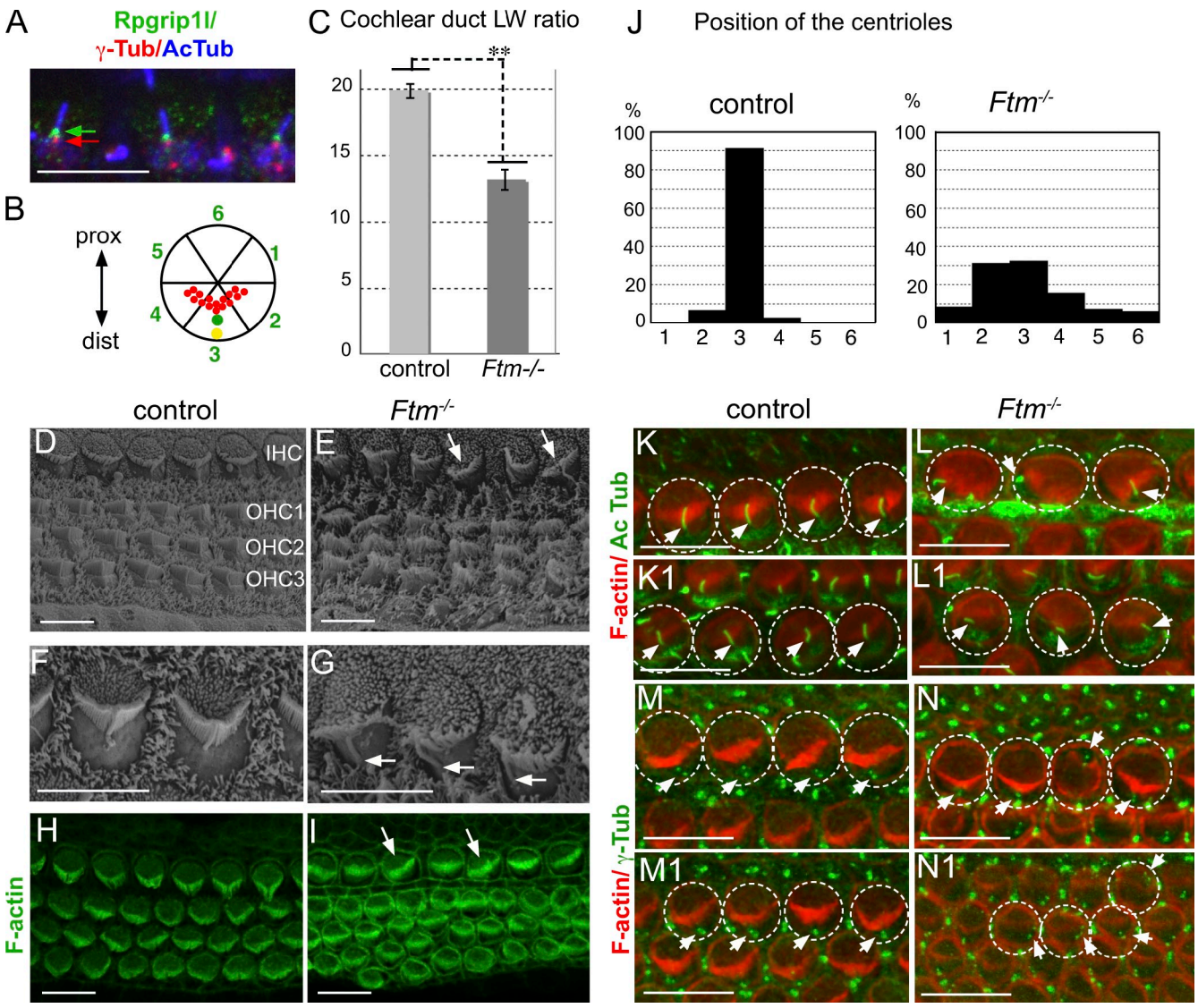

Figure 1. ***Ftm* mouse mutants show planar polarity defects in the organ of Corti.** (A) Immunofluorescence (IF) on an E18.5 wild-type cochlea showing Rpgrip1l accumulation at the transition zone of the cilium (green arrow), between the basal body (red arrow) and the axoneme. (B) Schematic drawing of a wild-type sensory hair cell, showing the relative positions of the stereociliary bundle (red), the kinocilium basal body (green), and the daughter centriole (yellow). The green numbers (1–6) correspond to the six quadrants used to monitor the position of the kinocilium in J. The proximo-distal axis of the cochlea (inner-outer axis, PCP axis) is indicated. (C) Diagram illustrating the mean length/width (LW) ratio of flat-mounted cochlear ducts of E18.5 controls: ($Ftm^{+/+}$ or $Ftm^{+/-}$, $n = 20$) and $Ftm^{-/-}$ ($n = 18$) fetuses. Double asterisk indicates that the difference in mean LW ratio between control and $Ftm^{-/-}$ cochleae is significant (Student's t-test, $\alpha < 0.0005$). (D–G) Scanning electron microscopy on dissected cochleae of E18.5 control (D and F) and $Ftm^{-/-}$ (E and G) fetuses. The position of the row of inner hair cells (IHC) and of the three rows of outer hair cells (OHC1-3) is indicated in D. (H and I) Phalloidin staining of F-actin on E18.5 control (H) and $Ftm^{-/-}$ (I) cochleae. (J) Diagrams showing the position of the centrioles in different cell quadrants illustrated in B. The normal position in wild-type cells is in quadrant 3. 123 control cells (three fetuses from three experiments) and 84 $Ftm^{-/-}$ cells (three fetuses from three experiments) were analyzed. The difference between control and $Ftm^{-/-}$ cells in the distribution of the centrioles in the different cell quadrants is significant (Khi2 test: $\alpha < 0.001$). (K–N1) Detection of acetylated α-tubulin (K–L1) or γ-tubulin (M–N1) and F-actin in E18.5 control (K, K1, M, and M1) or $Ftm^{-/-}$ (L, L1, N, and N1) cochleae. K, L, M, and N: IHCs; K1, L1, M1, and N1: OHCs. In selected cells (circled), white arrows point to the position of cilia (K–L1) or centrioles (M–N1). In all the pictures, proximal is to the top. Bars, 5 µm. Antibodies are indicated and color coded. All pictures and measurements were performed in the basal 25% of the cochlea.

cells in the *Ftm* mouse mutant line, which harbors a null mutation in the *Ftm/Rpgrip1l* gene (Vierkotten et al., 2007). Because *Ftm* mice die at birth, cochlear defects were analyzed in E18.5 fetuses, when PCP is already established in the cochlea. $Ftm^{-/-}$ cochleae were slightly shorter than that of control ($Ftm^{+/+}$ or $Ftm^{+/-}$) fetuses (Fig. 1 C), suggesting a mild CE defect. The four rows of hair cells were slightly disorganized, with additional hair cells between the three rows of outer hair cells (OHCs; Fig. 1, H and I). In scanning electron microscopy, the stereociliary hair bundles appeared less cohesive and did not present the normal V shape (Fig. 1, B and D–G). Misorientation of the hair bundles was observed in few cells (Fig. 1 E, arrows). This was confirmed and quantified by staining F-actin with phalloidin (Fig. 1, H and I). At the base of $Ftm^{-/-}$ cochleae, 4.8% of sensory cells had a misoriented bundle (over 30° of angle deviation; Fig. 1 I, arrows) and 2.5% had a round bundle ($n = 522$

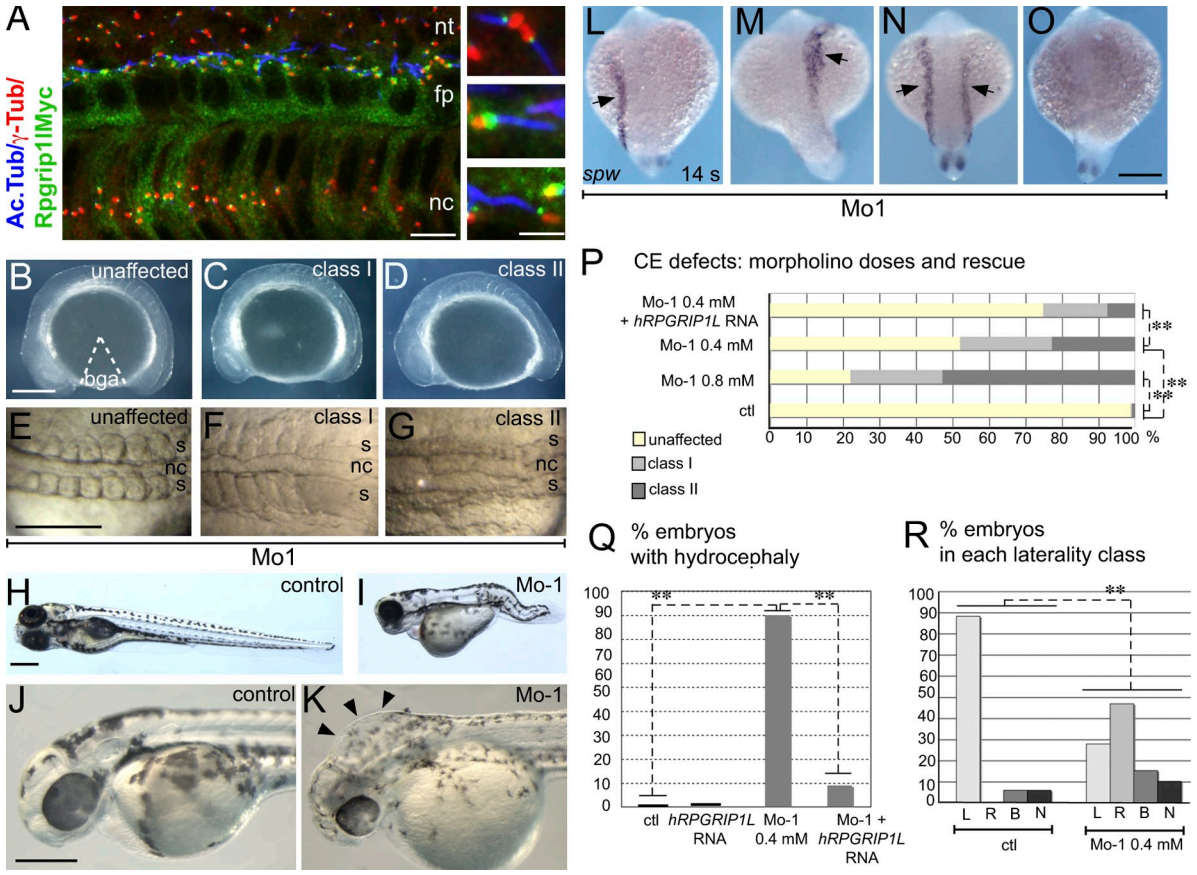

Figure 2. ***Rpgrip1l* depletion in zebrafish embryos leads to CE defects, hydrocephaly, and impaired laterality.** (A) IF on embryos injected with an RNA coding for a tagged form of Rpgrip1l (Rpgrip1l-Myc), showing its localization at the transition zone of the cilium in the neural tube (nt), floor plate (fp), and notochord (nc). Enlarged views of selected cilia are presented in insets on the right. (B–D) *Rpgrip1l* morpholino-injected embryos (Mo-1) at the 12-s stage, representative of the three phenotypic classes: unaffected (B, indistinguishable from uninjected controls, body gap angle [bga] around 50°), class I (C, mild, 60° < bga < 90°, kinked notochord, and class II (D, severe: 90° < bga < 120°, malformed somites and kinked, broader notochord). (E–G) dorsal views of representative embryos of the three classes, showing the kinked notochord (nc) and malformed somites (s) in class I/II embryos. (H and I) 5-dpf control (H) and *rpgrip1l* morphant (I) larvae, showing the shortened and abnormally curved trunk in morphants. (J and K) Lateral views of 48-hpf control (J) and *rpgrip1l* morphant (K) embryos showing hydrocephaly in morphants (K, arrowheads). (L–O) Laterality defects in *rpgrip1l* morphants. *southpaw* (*spw*) expression patterns in the lateral mesoderm (arrows), visualized by ISH, fall into four different classes: left, right, bilateral, and absent. (P) Diagrams illustrating the axis elongation phenotype. For each class (color coded), the percentage of embryos is indicated by the length of the horizontal bars. The number of embryos scored is 236 for uninjected (ni), 159 for 1 mM Mo-Rpgrip1l, 408 for 0.4 mM Mo-Rpgrip1l, and 171 for 0.4 mM Mo-Rpgrip1l + *hRPGRIP1L* RNA. Double asterisk indicates that the difference in the distribution of embryos in the different phenotypic classes is significant (Khi2 test: $\alpha < 0.001$). The morphant phenotype is dependent on the dose of morpholino (0.4 vs. 0.8 mM; 1 mM corresponds to 1 pmol/embryo) and is partially rescued by co-injection of human *RPGRIP1L* mRNA (100 pg). (Q) Diagram illustrating the percentage of hydrocephalic embryos. Number of embryos scored: 32 for uninjected, 32 for *hRPGRIP1L* RNA, 25 for 0.8 mM Mo-1 + *GFP* RNA, and 22 for 0.8 mM Mo-1 + *hRPGRIP1L* RNA. **, $\alpha < 0.001$, Khi2 test. (R) Diagram indicating the number of control and morphant embryos in each of the laterality classes illustrated in L–O: left (L), right (R), bilateral (B), and no expression (N). Number of embryos scored: 17 for uninjected, 79 for 0.4 mM Mo-1. **, $\alpha < 0.001$, Khi2 test. In Q and R, the data shown are from a single representative experiment out of two (Q) or four (R) repeats, respectively. Bars: (A) 10 µm; (A, insets) 2.5 µm; (B–O) 250 µm.

cells from 4 $Ftm^{-/-}$ fetuses), whereas control cells had 1% misoriented and no round bundles (n = 595 cells from 5 control fetuses). In control cochleae, the kinocilium is positioned at the vertex of the hair bundle (Fig. 1, B, K, and K1) and is connected to the stereocilia by extracellular links (Jones and Chen, 2008). In $Ftm^{-/-}$ cochleae, the kinocilium was incorrectly positioned and oriented, and was disconnected from the stereociliary bundle (Fig. 1, G, L, and L1). In addition, ciliogenesis was impaired in a small proportion of cells: the kinocilium was either shorter in 16% or absent in 12% of the cells (n = 193; Fig. 1, L and L1). We then performed γ-tubulin staining in order to accurately position the two centrioles within the cells. In control hair cells, the two centrioles were close to each other and aligned along the proximo-distal axis (n = 122 cells from 3 control fetuses) (Fig. 1, B, J, M, and M1). In two thirds of hair cells in $Ftm^{-/-}$ cochleae, the centrioles were not in the distal quadrant and/or not properly aligned along the proximo-distal axis (n = 83 cells from 3 $Ftm^{-/-}$ fetuses; Fig. 1, J, N, and N1). In rare cases (2 of 100 cells), the two centrioles were far from each other. Our results on kinocilium and centriole position defects in hair cells of $Ftm^{-/-}$ cochleae indicate a role for Rpgrip1l in PCP.

Zebrafish *rpgrip1l* morphants display planar polarity defects

To further study the involvement of Rpgrip1l in PCP, we turned to the zebrafish model. We identified a single orthologue of the human *RPGRIP1L* gene in the zebrafish genome (Ensembl prediction GenBank/EMBL/DDBJ accession no. XM_002666951)

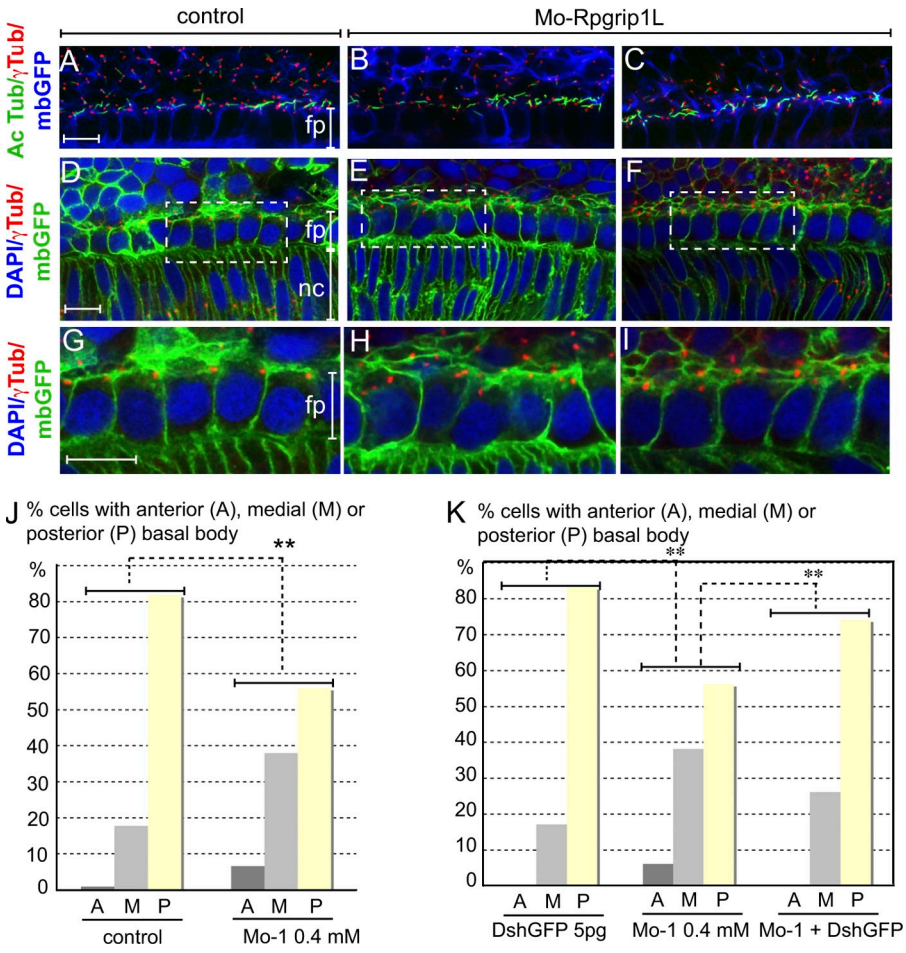

Figure 3. **Rpgrip1l is necessary for posterior positioning of the basal body in floor plate cells.** (A–F) Lateral confocal sections of 18-s stage control (A, D, and G) and *rpgrip1l* morphant (B, C, E, F, H, and I) embryos stained with antibodies to acetylated α-tubulin (A–C), γ-tubulin, and GFP. The embryos have been injected at the 1-cell stage with an *mbGFP* RNA in order to visualize cell membranes. G, H, and I are higher magnifications of the regions boxed in D, E, and F, respectively. (J and K) Diagrams illustrating the percentage of floor plate cells with a basal body in posterior (P), medial (M), or anterior (A) position in 18-s stage control embryos (J) or after injection of 4 ng/µl *Dsh-GFP* RNA (K), 0.4 mM Mo-Rpgrip1l (J and K), or co-injected with both (K). The diagram in J corresponds to 2 independent injection experiments with a total of 7 controls (142 cells analyzed) and 14 *rpgrip1l* morphants (172 cells analyzed). The diagram in K corresponds to 2 independent injection experiments with a total of 8 controls (130 cells analyzed), 11 *rpgrip1l* morphants (183 cells analyzed), and 11 morphants co-injected with *Dsh-GFP* mRNA (168 cells). The double asterisks in J and K mean that the differences in the distributions of the three phenotypic classes between the compared experimental conditions are statistically significant (Khi2 test: $\alpha < 0.001$). In A–I, anterior is to the left and dorsal is up. In D–I, a single confocal section is shown. Bars, 10 µm in all pictures.

and determined its full-length coding sequence (GenBank accession no. JN051142). The zebrafish *rpgrip1l* gene encodes a 1259-amino acid protein with 51% identity and 67% similarity with the human RPGRIP1L protein. Zebrafish *rpgrip1l* is expressed both maternally and zygotically, widely at early somite stages, then mainly in the central nervous system after 24 hours post-fertilization (hpf; Fig. S1). Injection of RNA coding for a tagged form of Rpgrip1l revealed that the protein was enriched in the transition zone of the cilium in all monociliated cell types examined, including the neural tube, floor plate, and notochord cells (Fig. 2 A). We next performed *rpgrip1l* loss-of-function experiments using two antisense morpholinos, targeting the translation start site (Mo-1) and a region 55–31 nucleotides upstream of the translation start site (Mo-55). Morphological examination of the morphants showed shortened body axis, kinked notochord/neural tube, and malformed somites at early somite stages, abnormal body curvature after 24 hpf, and hydrocephaly at 2 dpf (Fig. 2, B–K). The embryos were separated into three classes depending on the severity of the axis elongation phenotype, as measured by the body gap angle (bga; angle between the tip of the head and the tip of the tail) at the 10–12-s stage (Fig. 2, B–D and P). Morphants that survived up to 5 dpf were shorter and had a curved body (Fig. 2, H and I), as found in PCP mutants (Jessen et al., 2002). Shorter axis and curved body strongly suggested the existence of CE defects, which was confirmed using molecular landmarks (Fig. S2, A–F). The number and size of cilia, the localization of several ciliary proteins within the cilium shaft, and the structure of basal bodies appeared unchanged in most tissues of *rpgrip1l* morphants as compared with controls (Fig. 3, A–C; and Fig. S2, G–Q). Because both morpholinos gave similar and dose-dependent phenotypes, more robust with Mo-1 than with Mo-55 (unpublished data), Mo-1 was used in most experiments (hereafter called Mo-Rpgrip1l). Co-injection of human *RPGRIP1L* mRNA with the morpholinos rescued the CE phenotype, with a significant decrease in the number of affected embryos and the severity of the defects (Fig. 2 P), as well as hydrocephaly (Fig. 2 Q), demonstrating that these defects were specific for the loss of Rpgrip1l function. *Rpgrip1l* morphants also displayed defective left–right asymmetry, as illustrated by randomized expression of the early laterality marker *spw* in the lateral plate mesoderm at 14 s (17 hpf; Fig. 2, L–O and R). Thus, *rpgrip1l* morphants display a ciliary phenotype characterized by abnormal CE and laterality, without general ciliary defects, allowing us to study Rpgrip1l function in planar polarity independently of its role in ciliogenesis.

In addition to CE, another manifestation of PCP in the early zebrafish embryo is the posterior position of the basal body in floor plate cells, which defects are associated with aberrant motile cilia tilting (Borovina et al., 2010). Because *rpgrip1l* transcripts are enriched in floor plate cells, we investigated its function in this process. In control embryos from the 14-s stage onward, 80% of the cells presented posterior basal bodies, as

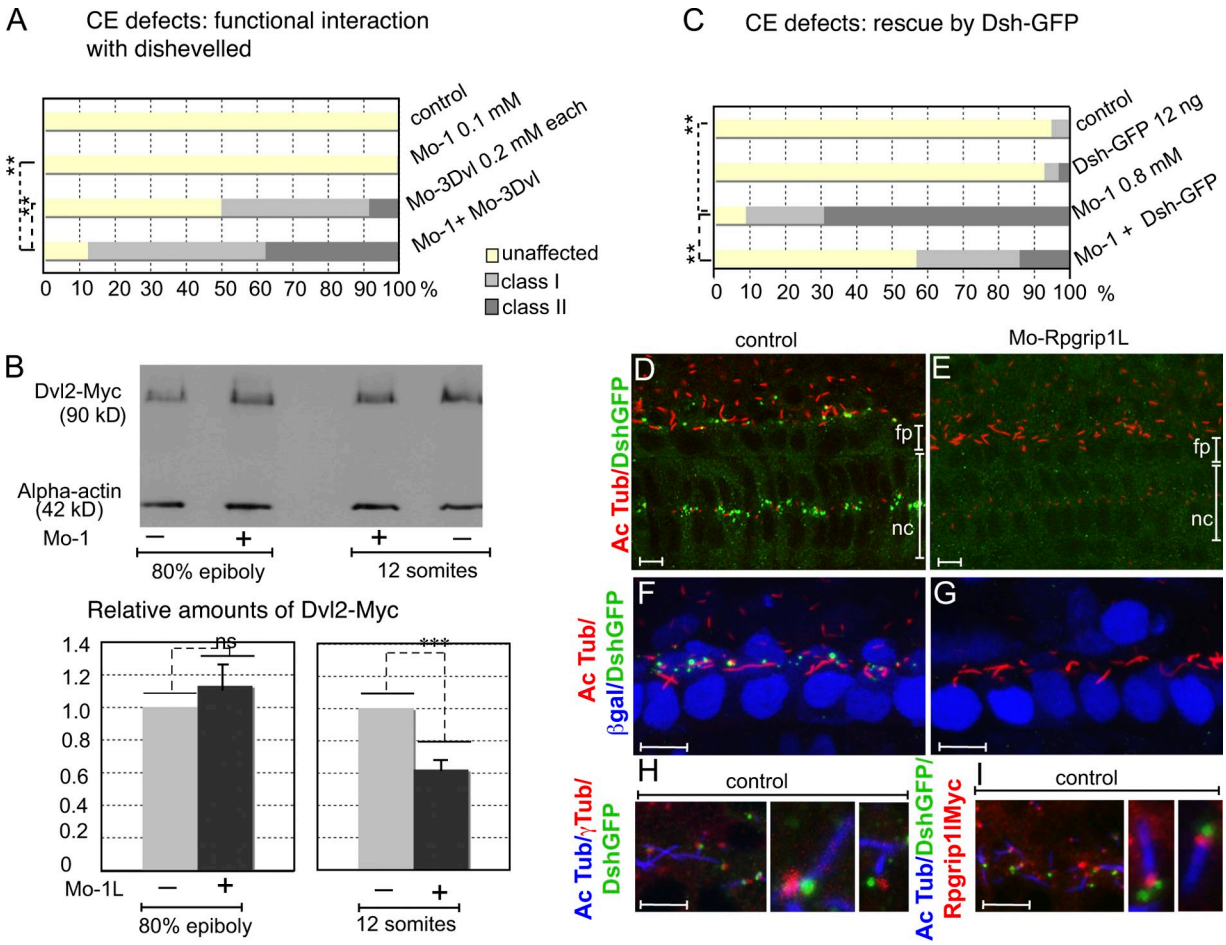

Figure 4. **Rpgrip1l stabilizes dishevelled at the cilium base.** (A) Diagram illustrating the functional interaction between Rpgrip1l and dishevelled in axis elongation. For each lane, the injected morpholinos are indicated on the right. *n* = 37 control, 29 Mo-Rpgrip1l–injected, 37 Mo-3Dvl–injected, and 24 co-injected embryos. The differences in the repartition in classes between batches of embryos injected with one morpholino only and the batch of co-injected embryos are significant ($\alpha < 0.001$, Khi2 test). (B) Western blots illustrating the amounts of Dvl2-Myc protein after injection of 15 pg *Dvl2-Myc* RNA per embryo at the 1-cell stage with or without co-injecting Mo-Rpgrip1l (0.8 mM). The diagrams illustrate the relative amounts of Dvl2-Myc in control and Mo-Rpgrip1l–injected embryos at the 80% epiboly and at the 12-s stages, in six independent experiments. Dvl amounts are in arbitrary units and the average amounts in control embryos are arbitrarily set at 1.0. (C) Diagram illustrating the axis elongation phenotype in embryos injected with Mo-Rpgrip1l and/or with *Dsh-GFP* RNA (12 ng/µl, corresponding to 12 pg/embryo). *n* = 23 control, 23 *Dsh-GFP* injected, 24 Mo-Rpgrip1l–injected, and 58 doubly injected embryos. *Dsh-GFP* mRNA (12 pg/embryo) significantly rescues the morphant phenotype ($\alpha < 0.001$, Khi2 test). (D and E) IF with an anti-GFP antibody to reveal the GFP tagged Dsh protein and with an anti-acetylated α-tubulin antibody (Ac Tub) to label cilia in embryos injected with *Dsh-GFP* (10 pg/embryo) with (E) or without (D, controls) Mo-Rpgrip1l (0.8 mM). (F and G) View of the floor plate after IF with anti-GFP, anti-βgal, and anti–Ac-Tub antibodies in 18-s stage embryos injected with *DshGFP* (10 pg/embryo) and *nlsLacZ* RNAs (60 pg/embryo) with (G) or without (F, controls) Mo-Rpgrip1l. anti-βgal staining in nuclei indicates that the corresponding cells have received injected RNA. (H) IF with anti–Ac-Tub, anti-GFP, and anti–γ-Tub antibodies in embryos injected with *Dsh-GFP* RNA alone. (I) IF with anti-GFP, anti-Myc, and anti–γ-Tub antibodies in embryos injected with *Dsh-GFP* (10 pg/embryo) and *Rpgrip1l-Myc* (7 pg/embryo) RNAs. Bars, 10 µm.

assessed by γ-tubulin staining in embryos injected with membrane-associated GFP to detect cell membranes (Fig. 3, D, G, and J). In *rpgrip1l* morphants, the posterior bias in basal body position was significantly reduced (Fig. 3, E, F, H, I, and J). These data demonstrate that Rpgrip1l is required for positioning the cilium along the antero-posterior (planar polarity) axis in the zebrafish floor plate.

Rpgrip1l acts in PCP by stabilizing dishevelled

We analyzed the functional interaction of *rpgrip1l* with several PCP genes and with *inversin* by performing combined knockdown in zebrafish embryos. Co-injection of low doses of Mo-Rpgrip1l with morpholinos specific for *vangl2* (Mo-Vangl2), *prickle1* (Mo-Pk1), for all three zebrafish *dvl* genes (Mo-3Dvl; Ségalen et al., 2010), or for *inv* (Mo-inv; Sayer et al., 2006) led to an increase in the severity of the axis elongation phenotype as compared with individual morphants (Fig. 4 A and Fig. S3, A–C). These results suggest either that Rpgrip1l and these proteins functionally interact during zebrafish CE, or that they act in parallel to promote common cellular processes.

Because dishevelled is a major actor of the Wnt pathways whose stability is modulated by the Rpgrip1l interactors nephrocystin-4 and inversin (Simons et al., 2005; Burcklé et al., 2011), we investigated a direct role of Rpgrip1l on its stability. For that purpose, we co-injected an RNA coding for a Myc-tagged form of *Xenopus* Dvl2 with Mo-Rpgrip1l into zebrafish embryos and analyzed by Western blots the amounts of Dvl2-Myc protein

recovered at different stages (Fig. 4 B). The amounts of Dvl2-Myc were not significantly different between control and *rpgrip1l* morphants at 80% epiboly (8.5 hpf). However, at 12 s (15 hpf), *rpgrip1l* morphants displayed a 40% reduction in Dvl2-Myc levels compared with controls, suggesting that Rpgrip1l stabilized dishevelled. Dvl protein levels are known to be important for zebrafish CE (Angers et al., 2006) and the knock-down of all three zebrafish *dvl* genes led to defects in asymmetric basal body localization in floor plate cells (Fig. S3 D). To test whether Rpgrip1l function in PCP is mediated by dishevelled stabilization, we performed a rescue experiment by co-injecting Mo-Rpgrip1l together with an RNA coding for a GFP-tagged form of *Drosophila* dishevelled (Dsh-GFP). This led to a significant rescue of the CE phenotype (Fig. 4 C), as well as of the posterior localization of basal body in floor plate cells (Fig. 3 K). Together, these data show that in these two processes, Rpgrip1l acts at least in part by stabilizing dishevelled.

Rpgrip1l localizes dishevelled to the basal body of zebrafish floor plate cells

To test whether dishevelled stability was affected uniformly in the embryo, or differentially in specific cell types or subcellular compartments, we performed whole-mount GFP immunofluorescence on embryos injected with *Dsh-GFP* mRNA. *NLSLacZ* mRNA, which codes for a nuclear form of β-galactosidase (βgal), was co-injected as a control of the presence of injected RNA in the cells. In control embryos at 12 s, Dsh-GFP concentrated in many cell types including the floor plate and notochord cells, in apical granules located at or close to the cilia (in 61% of the injected embryos, $n = 39$; Fig. 4 D). In double staining for βgal and GFP, all of the βgal-positive cells ($n = 86$ cells, 9 embryos) in the floor plate displayed Dsh-GFP granules at the cilium base, in the immediate vicinity of the basal body (Fig. 4, F and H). Co-injection of *Dsh-GFP* with *Rpgrip1lMyc* mRNA did not reveal colocalization between GFP and Myc, indicating that the dishevelled and Rpgrip1l proteins were enriched in adjacent structures at the cilium base (Fig. 4 I). In 95% of *rpgrip1l* morphants ($n = 41$), Dsh-GFP granules were either absent or severely reduced in number and size (Fig. 4 E) and found at the base of the cilium in only 9% of the βgal-positive cells ($n = 78$, 7 embryos; Fig. 4 G). In contrast, in *inv* morphants the cytoplasmic pool of Dsh-GFP was increased and the basal body pool was not grossly affected. In combined *inv, rpgrip1l* morphants the ciliary pool of Dsh-GFP was absent and the cytoplasmic pool was still present although reduced compared with *inv* morphants (Fig. S3, E–J). A Vangl2-GFP fusion protein showed a different behavior, with a homogenous localization at cell membranes in both controls and *rpgrip1l* morphants (Fig. S3, K–R). Together, these experiments strongly suggest that Rpgrip1l is required to maintain dishevelled levels in zebrafish floor plate cells and that it acts primarily but not exclusively on a pericentriolar pool of dishevelled.

Rpgrip1l stabilizes dishevelled at the cilium base of mammalian kidney cells

Overexpressed dishevelled protein tends to form aggregates whose physiological significance is unclear (Schwarz-Romond et al., 2005). To investigate Rpgrip1l function in the localization of endogenous dishevelled, we used polarizing monociliated MDCK cells, in which we have previously shown the endogenous expression of Dvl2, Dvl3, and RPGRIP1L at the base of the cilium (Burcklé et al., 2011). To test whether *RPGRIP1L* was required for dishevelled localization, we generated stable *RPGRIP1L* knock-down MDCK cell lines with two different shRNA sequences (RPGRIP1L-KD-sh1/2). Silencing of *RPGRIP1L* led to ∼40% residual expression of mRNA and protein expression compared with control cell lines, as assessed by quantitative RT-PCR and Western blotting (Fig. S4 A). In both RPGRIP1L-KD cell lines, RPGRIP1L depletion resulted in a reduction of both the number and the length of cilia, as well as in a disruption of the pericentriolar material (Fig. S4, B–D). We then examined whether endogenous dishevelled localization was altered upon RPGRIP1L depletion. In most polarizing control MDCK cells, Dvl2 and Dvl3 were detected in and around the basal body, and sometimes in the cytoplasm (Fig. 5 A, diagrams). In contrast, Dvl2 or Dvl3 pericentriolar staining was lost or severely reduced in a large majority (75–80%) of RPGRIP1L-depleted cells (Fig. 5 A). This correlated with a global reduction in total Dvl2 and Dvl3 protein amounts, without modification of mRNA levels (Fig. 5, B and C), suggesting that Rpgrip1l stabilizes dishevelled proteins in these cells. The decrease in Dvl2 and Dvl3 levels at the basal body was rescued upon reexpression of RPGRIP1L-Myc in RPGRIP1L-KD cells (Fig. S5, A–C). Using other experimental conditions allowing the detection of Dvl2 and Dvl3 at the cell membrane, we showed that the membrane localization of dishevelled was still observed after RPGRIP1L depletion (Fig. S5 D). Because inversin and nephrocystin-4 have been shown to bind and destabilize dishevelled (Simons et al., 2005; Burcklé et al., 2011), we tested whether RPGRIP1L depletion prevented their localization at the base of the cilium. RPGRIP1L depletion led to a reduction of the pericentriolar accumulation of inversin and nephrocystin-4 along with a disruption of γ-tubulin staining in ∼50% of the cells. However, in the 50% of RPGRIP1L-KD cells where γ-tubulin staining remained, inversin and nephrocystin-4 as well as two other ciliopathy proteins, nephrocystin-3 and CEP290, accumulated around the basal body, similar to control MDCK cells (Fig. 5, D and E; and Fig. S4, D–G). These results suggest that RPGRIP1L depletion in these cells leads to a drastic and widespread reduction of Dvl accumulation at the cilium base, which partially correlates with a destabilization of the pericentriolar material.

Rpgrip1l acts in a complex with inversin and nephrocystin-4 to modulate dishevelled stability

We next investigated the mechanisms by which RPGRIP1L stabilizes dishevelled. Inhibition of the proteasome by treatment of RPGRIP1L-KD cells with clasto-lactacystin led to a rescue of Dvl3 amounts to levels comparable to that found in control PSICOR cells (Fig. 6 A), strongly suggesting that RPGRIP1L stabilizes dishevelled by preventing its proteasomal degradation. To determine whether RPGRIP1L is sufficient for dishevelled stabilization, we overexpressed RPGRIP1L-Myc in HEK293T

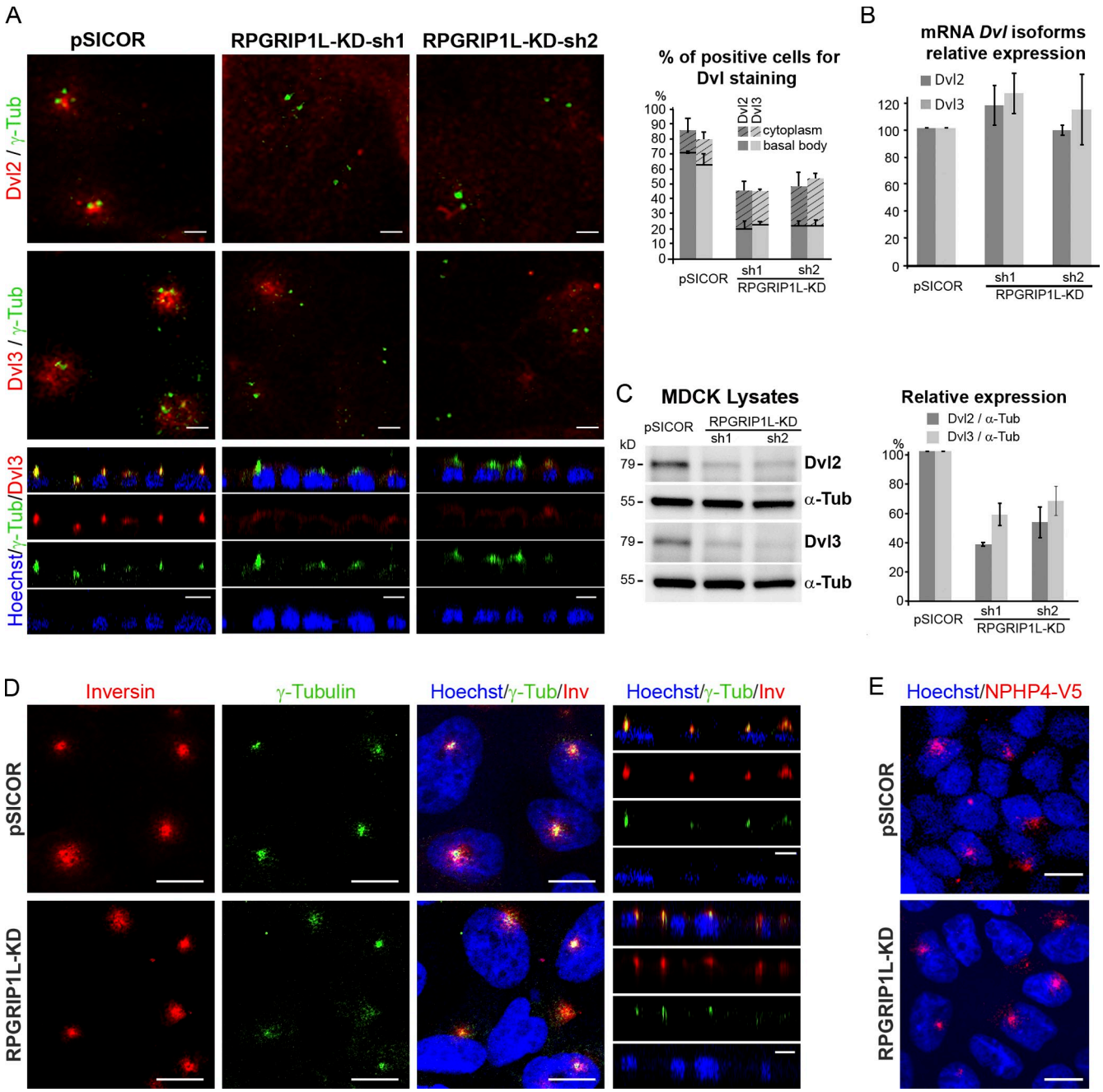

Figure 5. **RPGRIP1L stabilizes dishevelled at the cilium base in cultured mammalian renal cells.** (A) Co-immunostaining of Dvl2 (top) or Dvl3 (middle) with γ-tubulin on control and RPGRIP1L-KD MDCK cells. The bottom panel shows z-section of coimmunostaining of Dvl3 and γ-tubulin in the three cell lines. The histogram compares the percentage of cells with Dvl2 or Dvl3 staining and their accumulation in the pericentriolar region versus the cytoplasm (800–900 cells analyzed). (B) Quantitative RT-PCR analysis of *Dvl2* and *Dvl3* mRNA levels in control and RPGRIP1L-KD MDCK cells. (C) Western blot analysis and quantification of endogenous Dvl2 and Dvl3 in control and RPGRIP1L-KD MDCK cells. (D) Coimmunostaining of inversin with γ-tubulin on control and RPGRIP1L-KD MDCK cells. The right panel shows z-section of the stainings in both cell lines. (E) Immunostaining of NPHP4-V5 on control and RPGRIP1L-KD MDCK cells transduced with the *NPHP4-V5* expression construct (Burcklé et al., 2011). In A, D, and E nuclei were stained with Hoechst. Bars: (C, D, z-sections A or C) 10 µm; (A, top and middle panels) 2 µm.

cells and compared its effect to that of inversin-Flag (Inv-Flag) overexpression. Whereas inversin overexpression strongly decreased Dvl2-Myc protein levels, RPGRIP1L-Myc overexpression led to a significant increase in Dvl2-Myc levels (Fig. 6 B).

To determine whether RPGRIP1L, inversin, nephrocystin-4, and dishevelled could act together in a same complex or whether Rpgrip1l would compete with inversin and nephrocystin-4 for dishevelled binding, we performed coimmunoprecipitation experiments in HEK293T cells with tagged forms of these proteins. We found that inversin coimmunoprecipitated both RPGRIP1L and Dvl2, and that coexpression of RPGRIP1L and Dvl2 with inversin increased the levels of immunoprecipitated Dvl2, in a manner consistent with the stabilization of Dvl2 by RPGRIP1L in total lysates (Fig. 6 C). Moreover, when coexpressed, nephrocystin-4 coimmunoprecipitated both Dvl2 and RPGRIP1L (Fig. 6 D). We next tested in this assay dishevelled stabilization by mutant forms

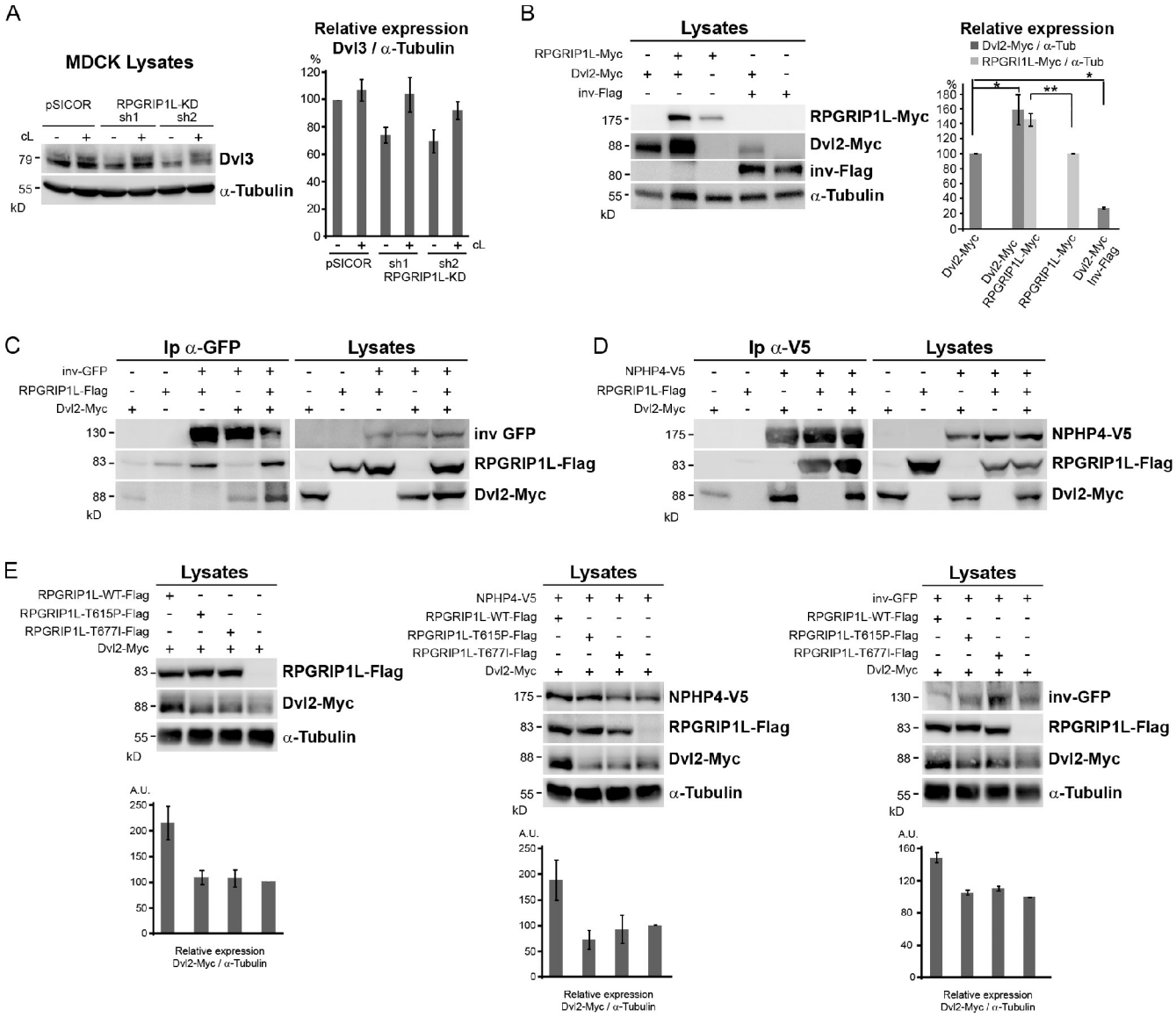

Figure 6. **Rpgrip1l forms a complex with dishevelled, inversin, and nephrocystin-4.** (A) Western blot analysis and quantification of endogenous levels of Dvl3 in control and RPGRIP1L-depleted MDCK cells. The reduction observed in RPGRIP1L-KD was blocked by the proteasome inhibitor clasto-lactacystin β-lactone (cL). Western blot was reprobed for α-tubulin as a loading control ($n = 3$). (B) Western blot analysis and quantification of Dvl2-Myc expression levels. HEK293T cells were transiently transfected with a Dvl2-Myc expression construct alone or together with either RPGRIP1L-Myc or Inv-Flag expression constructs ($n = 4$). *, $P < 0.03$; **, $P < 0.002$; Mann Whitney test. (C and D) Dvl2-Myc and RPGRIP1L-Flag were coexpressed with inv-GFP (C) or V5-tagged NPHP4 (D, NPHP4-V5) in HEK293T cells. After immunoprecipitation with anti-GFP (C) or anti-V5 (D), both Dvl2-Myc and RPGRIP1L-Flag were specifically detected in immunoprecipitates (C and D, left panels). Expression level of transfected proteins in cell lysates was confirmed by immunoblotting with appropriate antibodies (C and D, right panels). (E) Western blot analysis and quantification of Dvl2-Myc expression levels. HEK293T cells were transiently transfected with a Dvl2-Myc expression construct alone or together with RPGRIP1L-Flag or RPGRIP1L-Flag with patient mutation (RPGRIP1L-T615P-Flag or RPGRIP1L-T677I-Flag). While RPGRIP1L-Flag construct stabilized Dvl2-Myc expression, constructs with patient mutation had a reduced efficiency (left panels). Then HEK293T cells were transiently transfected with a Dvl2-Myc expression construct together with either RPGRIP1L-Flag or RPGRIP1L-Flag with patient mutation and NPHP4-V5 (middle panels) or inv-GFP (right panels). Dvl2-Myc was not as efficiently protected from degradation when coexpressed with RPGRIP1L-Flag patient mutation constructs than the wild-type RPGRIP1L construct ($n = 3$).

of RPGRIP1L identified in cases of Joubert type B syndrome and known to interact less efficiently with nephrocystin-4 (Delous et al., 2007). We found that these mutant forms had a reduced capacity to stabilize Dvl2 (Fig. 6 E), consistent with their reduced capacity to rescue CE defects in zebrafish (Khanna et al., 2009).

Discussion

In this paper we investigated the function of the ciliopathy protein Rpgrip1l in planar polarity. We show that, in the mammalian cochlear sensory epithelium and in the zebrafish floor plate, Rpgrip1l is required for correct positioning of the basal body along the PCP axis. We demonstrate that Rpgrip1l is essential for stabilizing dishevelled in different experimental systems and that in the zebrafish floor plate this stabilization of dishevelled by Rpgrip1l mediates basal body positioning. Finally, our experiments in cell culture suggest that Rpgrip1l acts in a complex with nephrocystin-4 and inversin to finely regulate dishevelled stability.

Our data uncover a function for Rpgrip1l in several PCP processes characterized by a stereotyped position of the centrioles along the PCP axis (Jones and Chen, 2008; Borovina et al., 2010; Sepich et al., 2011). Rpgrip1l could act at several levels in these processes. It could be a general modulator of planar polarity, controlling the polarized localization of core PCP pathway proteins. Alternatively, it could be involved in interpreting a preexisting polarity information that would result in the asymmetric positioning of the basal body. Finally, it could act in parallel to and independently of the PCP pathway. Our results are not in favor of the first possibility. First, in cochleae, *Rpgrip1l* mutation leads to a mild disruption of the orientation of the stereociliary bundles, confirming that distinct planar polarity events in these cells can be uncoupled in ciliary mutants (Jones et al., 2008; Sipe and Lu, 2011). Moreover, the rescue of CE defects and of cilium positioning in the zebrafish floor plate by dishevelled shows that Rpgrip1l function is mediated at least in part by dishevelled stabilization. This places Rpgrip1l either downstream of, or in parallel to, cortical asymmetric cues, and upstream of intracellular basal body positioning. In the *Drosophila* wing (Goodrich and Strutt, 2011) as in the *Xenopus* skin (Mitchell et al., 2009), dishevelled acts cell-autonomously to establish polarity within cells, while Strabismus/Vangl and Frizzled transmembrane proteins also act in the coordination of planar polarity between adjacent cells. Thus, we propose that Rpgrip1l, by maintaining dishevelled levels, is specifically involved in one planar polarity process, i.e., the asymmetric localization of the basal body.

The function of dishevelled in basal body positioning in the zebrafish floor plate is consistent with what is described in the mouse node (Hashimoto et al., 2010). In the cochlea, dishevelled loss of function perturbs stereocilia orientation (Wang et al., 2006), whereas *Rpgrip1l* loss of function does not. In this system, dishevelled has been described in a cortical crescent located at the distal membrane of the hair cells, where the centrioles are anchored (Wang et al., 2006; Etheridge et al., 2008; Sipe and Lu, 2011). It would be very interesting to know whether Rpgrip1l is required for dishevelled stability in this system, and we are currently investigating this question. Also, dishevelled effectors in asymmetric basal body localization in the zebrafish floor plate remain to be identified. A candidate is Rac1, which is a downstream effector of dishevelled in other cellular contexts (Gao and Chen, 2010; Ishida-Takagishi et al., 2012), and whose inhibition prevents both posterior positioning of the basal body in node cells (Hashimoto et al., 2010) and positioning of the kinocilium on the distal side of cochlear hair cells (Sipe and Lu, 2011).

Our data point to a functional interaction between dishevelled and Rpgrip1l, which leads to dishevelled stabilization. What are the mechanisms of this functional interaction? Our experiments in HEK293T cells suggest that a physical interaction between Rpgrip1l, nephrocystin-4, inversin, and dishevelled can occur. The Rpgrip1l–dishevelled interaction is likely to be indirect, through a macromolecular complex comprising nephrocystin-4 and inversin (Simons et al., 2005; Delous et al., 2007; Burcklé et al., 2011). Rpgrip1l-dependent integrity of the cilium does not seem to be required because Rpgrip1l stabilizes dishevelled in HEK293T cells that do not form a cilium. We favor an alternative possibility, in which Rpgrip1l would be required for the stability and/or function of a pericentriolar platform involved in dishevelled stabilization. This is suggested by the reduction of the pericentriolar material and associated proteins in MDCK cells upon RPGRIP1L knock-down. Although Rpgrip1l is mainly found at the transition zone in many cell types, it is known to interact with pericentriolar proteins (Coene et al., 2011).

Several ciliopathy proteins, in particular the Rpgrip1l interactors inversin and nephrocystin-4, have been shown to target cytoplasmic dishevelled for proteasomal degradation (Simons et al., 2005; Burcklé et al., 2011; Wallingford and Mitchell, 2011). Here we show that, in contrast, Rpgrip1l protects dishevelled from proteasomal degradation. How is the balance in dishevelled stability achieved, and is the subcellular localization of the complex important for this balance? Our data show that Rpgrip1l does not compete with binding of nephrocystin-4 or inversin to dishevelled. Rpgrip1l could act by anchoring an inversin–nephrocystin-4–dishevelled complex to the basal body. Indeed, in *C. elegans* neurons, nephrocystin-4 localization at the ciliary transition zone depends on Rpgrip1l (Williams et al., 2011). Rpgrip1l could also modify the activity of nephrocystin-4 and inversin on dishevelled, allowing a precise tuning of dishevelled stability. The stoichiometry or the conformation of the different ciliary proteins in the complex, depending on the cellular context, could modulate the recruitment and/or the activity of proteins involved in proteasomal degradation. For instance, it could modulate the recruitment or activity of the ubiquitin ligase APC-C, which interacts with both dishevelled and inversin and regulates dishevelled stability (Morgan et al., 2002; Ganner et al., 2009). These two different mechanisms, localization of the complex to the pericentriolar region, and modulation of the activity of the complex, are not mutually exclusive and could both participate in fine-tuning dishevelled stability.

In conclusion, we describe here a novel, central function of an Rpgrip1l-dependent nephrocystin complex in stabilizing dishevelled, and we provide compelling evidence that this function is required for planar localization of the basal body. In mice, altered Wnt-PCP signaling results in kidney cysts appearing before birth, associated with CE defects in the elongating renal tubules (Karner et al., 2009). Thus, the function of Rpgrip1l in planar polarity may help interpret defects such as kidney dysfunctions found in mouse *Ftm* mutants and in humans presenting *RPGRIP1L* mutations. In this respect, our observation that *RPGRIP1L* mutations found in Joubert syndrome type B fail to stabilize dishevelled highlights possible physiopathological mechanisms occurring in ciliopathies.

Materials and methods

Mouse and zebrafish strains

Ftm mutant mice were maintained in a C57Bl6/J background and genotyped as described previously (Vierkotten et al., 2007). Embryonic day 0.5 (E0.5) was defined as noon on the day of vaginal plug detection. We used zebrafish wild-type AB or (TL x AB) hybrid strains and the Tg β-actin:: Arl13b-GFP transgenic line, which expresses a GFP fusion protein with the

ciliary protein Arl13b, under the control of the strong ubiquitous β-actin promoter (Borovina et al., 2010). Zebrafish were raised and maintained as described previously (Kimmel et al., 1995). Embryos were staged according to the number of hours (hpf) or days (dpf) post-fertilization at 28°C. Alternatively, for staging epiboly-stage embryos we used the percentage of yolk covered by the embryo (% epiboly); for somite-stage embryos, the number of somites was used (Kimmel et al., 1995).

Construction of Rpgrip1l expression plasmids

pCS2-RPGRIP1L (human) was constructed by transferring an EcoRI–XbaI fragment from pSPORT-RPGRIP1L, containing the whole human cDNA (Delous et al., 2007) into pCS2+. The zebrafish Rpgrip1l cDNA sequence was reconstructed from the IRAKp961G13289Q clone and RT-PCR fragments and was cloned into pCS2+. To obtain Myc-tagged zebrafish Rpgrip1l (Rpgrip1l-Myc), 5 Myc epitope tags were added in frame in the C terminus, removing the last 11 amino acids of the Rpgrip1l protein and the 3′-UTR.

Zebrafish microinjection

1 nL RNA- and/or morpholino-containing Daniau medium was injected into 1- to 4-cell stage embryos. *Rpgrip1l* translation-blocking morpholinos (Gene Tools) were designed to target either a region located at 1–24 bp downstream (Mo-1: 5′-AGTTTCATCAGCACGAGAAAACATC-3′) or 55–31 bp upstream (Mo-55: 5′-GACCACAGCGACAGTTGCTAAGAAA-3′) of the translation start site. For functional interaction studies, morpholinos targeting Vangl2 (5′-GTACTGCGACTCGTTATCCATGTC-3′; Otto et al., 2003), Prickle1 (5′-GCCCACCGTGATTCTCCAGCTCCAT-3′; Carreira-Barbosa et al., 2003), the three zebrafish Dvl (Dvl2: 5′-TAAATTATCTTGGTCTCC-GCCATGT-3′; Dvl2-like: 5′-GGTATATGATTTTAGTCTCCGCCAT-3′; Dvl3: 5′-GGTAGATAACTTTAGTCTCCCCCAT-3′; Ségalen et al., 2010), and inv (splice morpholino, 5′-GGACATAAGTACCTTCTCCATGCTC-3′; Sayer et al., 2006) were used. mRNA was synthesized in vitro from pCS2+ (or pSP6 for NLSLacZ) recombinant plasmids with the mMessage mMachine kit (Ambion) and injected at the following doses: *Dsh-GFP* (*Drosophila* dishevelled, 10 pg for subcellular localization, 12 pg for rescue experiments), *Ras-eGFP* (*mbGFP*: membrane localization signal of Ras protein fused to eGFP; 60 pg; Ségalen et al., 2010), *mbCherry* (two membrane localization signals fused to GFP; 25 pg; Megason and Fraser, 2003; Megason, 2009), *GFP-centrin1* (human centrin1; 15 pg), mouse *GFP-Vangl2* (mouse Vangl2; 25 pg), *Myc-Dvl2* (*Xenopus* Dvl2, 15 pg), human *RPGRIP1L* (100 pg), *rpgrip1l-myc* (7 pg), and *NLSLacZ* (60 pg; Smith and Harland, 1991). All fused proteins are full length unless otherwise stated, and the position of the tag in the name of the plasmid reflects the position in the fusion protein.

Establishment of lentiviral cell lines and transient transfections

shRNA constructs targeting the coil-coiled domain 3 (sh1) and 5 (sh2) of the canine RPGRIP1L mRNA sequences (sh1: 5′-GGATAGAATTAAT-GATTTA-3′, sh2: 5′-GCAAGATTATGAACTCAAA-3′) were designed and cloned into the lentiviral pSICOR vector, lentiviruses were produced in HEK293T cells, and MDCK type II cells were infected, as described previously (Delous et al., 2009). MDCK control and RPGRIP1L-KD cells were transduced with human full-length NPHP4-V5 C-terminal (Burcklé et al., 2011) and human full-length RPGRIP1L-Myc C-terminal cDNAs both cloned in pRRL.SIN.cPPT.PGK/WPRE vector (Zufferey et al., 1998). HEK293T cell transfections were performed as described previously (Delous et al., 2009). *inv-Flag* was provided by I. Drummond (Harvard Medical School, Charlestown, MA); *inv-GFP* was provided by A. Benmerah (INSERM U1016, Paris, France); *Dvl2-Myc* was provided by S. Sokol (Mount Sinai School of Medicine, New York, NY). In cotransfection experiments with partial *Rpgrip1l-Flag* N-terminal (*Rpgrip1l-Flag, Rpgrip1l-T615P-Flag* and *Rpgrip1l-T677I-Flag* were in pCMV3-Flag described previously in Delous et al. [2007]) and *Dvl2-Myc*, or with *inv-Flag* and *NPHP4-V5*, 55–72% of the cells were cotransfected.

Immunoprecipitations, Western blots, and proteasome inhibition

Immunoprecipitations and Western blots in renal cells were performed as described previously (Delous et al., 2009). In brief, cells were lysed for 10 min with lysis buffer (1% Triton X-100, 50 mm Tris-HCl, pH 7.5, 150 mm NaCl, and 1 mm sodium orthovanadate with complete protease inhibitor cocktail; Roche). Insoluble debris was removed by centrifugation at 14,000 *g* for 15 min. Proteins were detected with mouse anti-Myc (1:1,000; Santa-Cruz Biotechnology, Inc.), mouse anti-Flag (1:1,000; Sigma-Aldrich), rabbit anti-Flag (1:1,000; Sigma-Aldrich), mouse anti-V5 (1:1,000; AbD Serotec), mouse anti-GFP (1:1,000; Roche), mouse anti–α-tubulin (1:5:000; Sigma-Aldrich), rabbit anti-Dvl2 and anti-Dvl3 (1:1,000 and 1:500, respectively; Cell Signaling Technology), and rabbit anti-NPHP3 (this paper). Images were captured with a Fusion Fx7 system and quantified with Bio-1D software (Vilbert-Lourmat). To inhibit proteasome-dependent degradation in MDCK cells, cells grown for 8 d were treated overnight with 10 µm of clasto-lactacystin β-lactone (Sigma-Aldrich) before collection. Cells were harvested and lysed as described above. For Western blots with zebrafish embryos, pools of 15 embryos injected with *Dvl2-Myc* RNA ± Mo-Rpgrip1l were collected for Western blot analysis. Embryos were manually dechorionated. For 80% epiboly embryos, a hole was made with forceps into the yolk sac to remove the vitellus. Older embryos were transferred to 200 µl of deyolking buffer (55 mM NaCl, 1.8 mM KCl, and 1.25 mM NaHCO) by pipetting with a 200-µl tip to disrupt the yolk sac. Embryos were shaken 5 min at 1,100 rpm to dissolve the yolk. Cells were pelleted for 2 min at 1,800 rpm, resuspended in Laemmli buffer, and stored at −80°C (Link et al., 2006). The Myc epitope was detected by 9B11 monoclonal antibody (catalog no. 2276, 1:1,000; Cell Signaling Technology). α-Actin was used as a loading control (monoclonal antibody A4700, 1:1,000; Sigma-Aldrich).

Cochlear dissection, immunofluorescence, and scanning electron microscopy

Inner ears were dissected in cold PBS and fixed in fresh 4% PFA for 3 h at 4°C, after opening the oval window. Cochleae were then rinsed three times in cold PBS and pinned with minutia on a dissection dish. Cartilages surrounding the cochlea were removed with fine forceps. The Reissner's membrane was then peeled off to expose the sensory epithelium. Cochleae still attached to the vestibule were then transferred to a 2-ml Eppendorf tube (Montcouquiol et al., 2008). After a permeabilization step of 15 min in PBS, 0.1% Triton X-100 at 4°C, blocking was performed for 1 h at 4°C in PBS, 0.1% Triton X-100, 10% normal goat serum. Cochleae were incubated overnight with the following primary antibodies: mouse anti-acetylated tubulin (catalog no. T6793, 1:250; Sigma-Aldrich), mouse anti–γ-tubulin (catalog no. GTU-88, 1:1,000; Sigma-Aldrich), or rabbit anti-Rpgrip1l (Vierkotten et al., 2007), Phalloidin–Alexa Fluor 488 (Molecular Probes) was added to stain F-actin. All secondary antibodies were from Molecular Probes and diluted 1:400. After a final overnight wash at 4°C, cochleae were detached from the vestibule with fine forceps, after removing nervous connections and underlying mesenchyme. Cochlea were then transferred on a glass coverslip, mounted in Vectashield (Vector Laboratories) and imaged using a confocal microscope (model TCS SP5 II; Leica) using an HCX Plan Apochromat 63x/1.40–0.60 oil objective at room temperature. All channels were acquired by sequential scanning on LAS-AF software (Leica). For scanning electron microscopy (SEM), inner ears were removed from E18.5 heads in 1.22x PBS (pH 7.4) and fixed overnight with 2% glutaraldehyde in 0.61x PBS (pH 7.4) at 4°C. They were washed several times in 1.22x PBS, and cochleae were dissected as indicated above and postfixed for 15 min in 1.22x PBS containing 1% OsO4. Fixed samples were then prepared for SEM as described previously (Besse et al., 2011). Samples were observed under a scanning electron microscope (model S260; Cambridge) at 10 keV.

Immunofluorescence on MDCK cells

MDCK cells were plated at 1.5×10^5 cells on coverslips and grown for 8 d. Cells were fixed in 4% PFA in PBS for 20 min followed by treatment with 50 mM NH_4Cl for 10 min. For detection of pericentrin, cells were fixed in 4% PFA/Pipes (as described in Sang et al., 2011) and permeabilized 10 min with 0.2% Triton X-100 in PBS. For detection of Dvl2 and Dvl3 at the membrane, cells were fixed in cold methanol for 10 min. Cells were then treated with PBS, 0.1% Tween 20, 3% BSA, and 10% donkey serum for 30 min before incubating with the following primary antibodies: rabbit anti-Cep290 (catalog no. ab84870, 1:100; Abcam), rabbit anti-pericentrin (Covance), rabbit anti-NPHP3 (APN3, 1:100), anti-inversin (1:50;Abcam), mouse anti-V5 (1:200; AbD Serotec), mouse anti-acetylated α-tubulin (1:5,000; Sigma-Aldrich), rabbit anti-Dvl2 (1:50; Enzo Life Sciences), rabbit anti-Dvl3 (1:50; Abcam), and mouse anti–γ-tubulin (1:50; Sigma-Aldrich), and then incubating with appropriate Alexa Fluor (555 or 647)–conjugated secondary antibodies (Molecular Probes). Nuclei were stained with Hoechst. Confocal images were taken using a laser-scanning microscope system (LSM 750; Carl Zeiss) with a Plan Achromat 40x/1.3 oil DIC M27 or a Plan Achromat 63x/1.4 oil DIC M27 objective (Carl Zeiss).

Immunofluorescence and analysis of basal body localization in zebrafish embryos

Zebrafish embryos were fixed for 4 h at room temperature in 4% PFA, manually dechorionated, blocked in PBD (phosphate-buffered saline containing 1% DMSO, 1% bovine serum albumin, 0.3% Triton X-100, and

2% goat serum), and incubated overnight with primary antibodies and 2 h with secondary antibodies. Primary antibodies were mouse anti-GFP (catalog no. 1181440001, 1:100; Roche), polyclonal anti-GFP (1:500; Molecular Probes), mouse anti-acetylated tubulin (catalog no. T6793, 1:250; Sigma-Aldrich), mouse anti–γ-tubulin (catalog no. GTU-88, 1:1,000; Sigma-Aldrich), rabbit anti–β-galactosidase (catalog no. 55976, 1:500; Cappel), mouse anti-Myc 9B11 (catalog no. 2276, 1:200; Cell Signaling Technology), rabbit anti-Vangl2 (Montcouquiol et al., 2006), rabbit anti-DS red (catalog no. 632496, 1:500; Takara Bio Inc.), rabbit anti-MKS1 (catalog no. HPA021812, 1:100; Sigma-Aldrich), and rabbit anti-Cep290 (catalog no. ab84870, 1:100; Abcam). All secondary antibodies were from Molecular Probes and diluted 1:400. Nuclei were stained with DAPI (Invitrogen). Zebrafish embryos were flat-mounted in Vectashield mounting medium (Vector Laboratories) and imaged under a motorized microscope (model DM6000B; Leica). Confocal images were captured by a confocal microscope (model TCS SP5 II; Leica) using an HCX Plan Apochromat 63x/1.40–0.60 oil objective (3x zoom) at room temperature. All channels were acquired by sequential scanning on LAS-AF software (Leica). For basal body localization, we acquired lateral views of the whole region corresponding to the floor-plate of 18- or 14-s embryos previously injected with RNAs encoding a membrane-bound GFP. Each cell was divided into three regions (anterior, median, posterior) and the position of the basal body stained with γ-tubulin was processed with ImageJ software (1.37v; National Institutes of Health) using median filter command (value = 2.0) followed by a threshold and erode-dilate binary commands. After image treatment, basal bodies and cell membrane confocal planes were merged and the position of basal bodies in each floor plate cell was determined in z stack. Images shown correspond to one optic section of 0.29 µm. Contrast and brightness of images were adjusted using Photoshop software (Adobe).

RT-PCR and in situ hybridization

For RT-PCR analysis, sets of primers specific to canine *RPGRIP1L* (5′-TTGAAGCAGTGACCCAGAAGA-3′ and 5′-TGGTGCCATAGGCAATATCCT-3′) were designed. Whole-mount in situ hybridization was performed according to standard protocols and imaged on a stereomicroscope (model MZ16; Leica) equipped with a camera (model DFC 425; Leica).

Online supplemental material

Fig. S1 shows zebrafish *rpgrip1l* gene expression. Fig. S2 shows no apparent defect in dorso–ventral (DV) and antero–posterior (AP) patterning, and in cilium and basal body integrity, in *rpgrip1l* morphants. Fig. S3 shows interaction of *rpgrip1l* with PCP genes and with *inversin*. Fig. S4 shows cilium and basal body integrity in MDCK cells upon RPGRIP1L depletion. Fig. S5 shows RPGRIP1L depletion in MDCK cells: rescue and dishevelled localization at the membrane.

We thank B. Ciruna for providing the zebrafish Arl13b-GFP transgenic line, S. Sokol for the Dvl2-Myc construct, J. Axelrod for Dsh-GFP, J.-F. Riou for nlsLacZ, V. Lecaudey for centrin2-GFP, S. Megason for mbCherry, N. Peyrieras for ras-eGFP, and A. Benmerah for Inv-GFP. We thank R. Schwartzmann, J.-F. Gilles, the Cell Imaging and Flow Cytometry facility and the electron microscopy facility of the IFR83 (Paris, France), and N. Goudin and M. Garfa-Traoré from the imaging facilities of the IFR 94 (Paris, France) for precious help in microscopy and image analysis. We thank the fish and mouse facilities of the IFR83 (Paris, France) for efficient technical support. We are grateful to N. David, N. Spassky, C. Laclef, and F. Giudicelli for fruitful discussions and critical reading of the manuscript; and to L. Besse, M. Delous, and R. Benkirane for their participation in some of the experiments.

This work was supported by the Centre National de la Recherche Scientifique (CNRS), the Institut National de la Santé et de la Recherche Médicale (INSERM), the Université Pierre et Marie Curie, the Agence Nationale de la Recherche (S. Schneider-Maunoury and S. Saunier grant R07089KS, S. Schneider-Maunoury grant "Ciliainthebrain"), the Association pour la Recherche sur le Cancer (grants 4951XA0731F and SFI20101201851 to S. Schneider-Maunoury), the Fondation pour la Recherche Médicale ("Equipe FRM" grant DEQ20071210558 to S. Saunier), and the Association pour l'Utilization du Rein Artificiel (AURA). H.-M. Gaudé was the recipient of a PhD fellowship from the Société de Néphrologie and the Association pour l'Information et la Recherche sur les maladies Rénales Génétiques (AIRG).

S. Schneider-Maunoury and C. Vesque jointly directed the project.

Submitted: 2 November 2011
Accepted: 6 August 2012

References

Angers, S., C.J. Thorpe, T.L. Biechele, S.J. Goldenberg, N. Zheng, M.J. MacCoss, and R.T. Moon. 2006. The KLHL12-Cullin-3 ubiquitin ligase negatively regulates the Wnt-beta-catenin pathway by targeting Dishevelled for degradation. *Nat. Cell Biol.* 8:348–357. http://dx.doi.org/10.1038/ncb1381

Arts, H.H., D. Doherty, S.E. van Beersum, M.A. Parisi, S.J. Letteboer, N.T. Gorden, T.A. Peters, T. Märker, K. Voesenek, A. Kartono, et al. 2007. Mutations in the gene encoding the basal body protein RPGRIP1L, a nephrocystin-4 interactor, cause Joubert syndrome. *Nat. Genet.* 39:882–888. http://dx.doi.org/10.1038/ng2069

Badano, J.L., N. Mitsuma, P.L. Beales, and N. Katsanis. 2006. The ciliopathies: an emerging class of human genetic disorders. *Annu. Rev. Genomics Hum. Genet.* 7:125–148. http://dx.doi.org/10.1146/annurev.genom.7.080505.115610

Besse, L., M. Neti, I. Anselme, C. Gerhardt, U. Rüther, C. Laclef, and S. Schneider-Maunoury. 2011. Primary cilia control telencephalic patterning and morphogenesis via Gli3 proteolytic processing. *Development.* 138:2079–2088. http://dx.doi.org/10.1242/dev.059808

Borovina, A., S. Superina, D. Voskas, and B. Ciruna. 2010. Vangl2 directs the posterior tilting and asymmetric localization of motile primary cilia. *Nat. Cell Biol.* 12:407–412. http://dx.doi.org/10.1038/ncb2042

Burcklé, C., H.M. Gaudé, C. Vesque, F. Silbermann, R. Salomon, C. Jeanpierre, C. Antignac, S. Saunier, and S. Schneider-Maunoury. 2011. Control of the Wnt pathways by nephrocystin-4 is required for morphogenesis of the zebrafish pronephros. *Hum. Mol. Genet.* 20:2611–2627. http://dx.doi.org/10.1093/hmg/ddr164

Cardenas-Rodriguez, M., and J.L. Badano. 2009. Ciliary biology: understanding the cellular and genetic basis of human ciliopathies. *Am. J. Med. Genet. C. Semin. Med. Genet.* 151C:263–280. http://dx.doi.org/10.1002/ajmg.c.30227

Carreira-Barbosa, F., M.L. Concha, M. Takeuchi, N. Ueno, S.W. Wilson, and M. Tada. 2003. Prickle 1 regulates cell movements during gastrulation and neuronal migration in zebrafish. *Development.* 130:4037–4046. http://dx.doi.org/10.1242/dev.00567

Coene, K.L., D.A. Mans, K. Boldt, C.J. Gloeckner, J. van Reeuwijk, E. Bolat, S. Roosing, S.J. Letteboer, T.A. Peters, F.P. Cremers, et al. 2011. The ciliopathy-associated protein homologs RPGRIP1 and RPGRIP1L are linked to cilium integrity through interaction with Nek4 serine/threonine kinase. *Hum. Mol. Genet.* 20:3592–3605. http://dx.doi.org/10.1093/hmg/ddr280

Corbit, K.C., A.E. Shyer, W.E. Dowdle, J. Gaulden, V. Singla, M.H. Chen, P.T. Chuang, and J.F. Reiter. 2008. Kif3a constrains beta-catenin-dependent Wnt signalling through dual ciliary and non-ciliary mechanisms. *Nat. Cell Biol.* 10:70–76. http://dx.doi.org/10.1038/ncb1670

Deans, M.R., D. Antic, K. Suyama, M.P. Scott, J.D. Axelrod, and L.V. Goodrich. 2007. Asymmetric distribution of prickle-like 2 reveals an early underlying polarization of vestibular sensory epithelia in the inner ear. *J. Neurosci.* 27:3139–3147. http://dx.doi.org/10.1523/JNEUROSCI.5151-06.2007

Delous, M., L. Baala, R. Salomon, C. Laclef, J. Vierkotten, K. Tory, C. Golzio, T. Lacoste, L. Besse, C. Ozilou, et al. 2007. The ciliary gene RPGRIP1L is mutated in cerebello-oculo-renal syndrome (Joubert syndrome type B) and Meckel syndrome. *Nat. Genet.* 39:875–881. http://dx.doi.org/10.1038/ng2039

Delous, M., N.E. Hellman, H.M. Gaudé, F. Silbermann, A. Le Bivic, R. Salomon, C. Antignac, and S. Saunier. 2009. Nephrocystin-1 and nephrocystin-4 are required for epithelial morphogenesis and associate with PALS1/PATJ and Par6. *Hum. Mol. Genet.* 18:4711–4723. http://dx.doi.org/10.1093/hmg/ddp434

Dowdle, W.E., J.F. Robinson, A. Kneist, M.S. Sirerol-Piquer, S.G. Frints, K.C. Corbit, N.A. Zaghloul, G. van Lijnschoten, L. Mulders, D.E. Verver, et al. 2011. Disruption of a ciliary B9 protein complex causes Meckel syndrome. *Am. J. Hum. Genet.* 89:94–110. http://dx.doi.org/10.1016/j.ajhg.2011.06.003

Etheridge, S.L., S. Ray, S. Li, N.S. Hamblet, N. Lijam, M. Tsang, J. Greer, N. Kardos, J. Wang, D.J. Sussman, et al. 2008. Murine dishevelled 3 functions in redundant pathways with dishevelled 1 and 2 in normal cardiac outflow tract, cochlea, and neural tube development. *PLoS Genet.* 4:e1000259. http://dx.doi.org/10.1371/journal.pgen.1000259

Ezratty, E.J., N. Stokes, S. Chai, A.S. Shah, S.E. Williams, and E. Fuchs. 2011. A role for the primary cilium in Notch signaling and epidermal differentiation during skin development. *Cell.* 145:1129–1141. http://dx.doi.org/10.1016/j.cell.2011.05.030

Fischer, E., and M. Pontoglio. 2009. Planar cell polarity and cilia. *Semin. Cell Dev. Biol.* 20:998–1005. http://dx.doi.org/10.1016/j.semcdb.2009.09.016

Ganner, A., S. Lienkamp, T. Schäfer, D. Romaker, T. Wegierski, T.J. Park, S. Spreitzer, M. Simons, J. Gloy, E. Kim, et al. 2009. Regulation of ciliary

polarity by the APC/C. *Proc. Natl. Acad. Sci. USA*. 106:17799–17804. http://dx.doi.org/10.1073/pnas.0909465106

Gao, C., and Y.G. Chen. 2010. Dishevelled: The hub of Wnt signaling. *Cell. Signal.* 22:717–727. http://dx.doi.org/10.1016/j.cellsig.2009.11.021

Garcia-Gonzalo, F.R., K.C. Corbit, M.S. Sirerol-Piquer, G. Ramaswami, E.A. Otto, T.R. Noriega, A.D. Seol, J.F. Robinson, C.L. Bennett, D.J. Josifova, et al. 2011. A transition zone complex regulates mammalian ciliogenesis and ciliary membrane composition. *Nat. Genet.* 43:776–784. http://dx.doi.org/10.1038/ng.891

Gerdes, J.M., Y. Liu, N.A. Zaghloul, C.C. Leitch, S.S. Lawson, M. Kato, P.A. Beachy, P.L. Beales, G.N. DeMartino, S. Fisher, et al. 2007. Disruption of the basal body compromises proteasomal function and perturbs intracellular Wnt response. *Nat. Genet.* 39:1350–1360. http://dx.doi.org/10.1038/ng.2007.12

Goetz, S.C., and K.V. Anderson. 2010. The primary cilium: a signalling centre during vertebrate development. *Nat. Rev. Genet.* 11:331–344. http://dx.doi.org/10.1038/nrg2774

Goodrich, L.V., and D. Strutt. 2011. Principles of planar polarity in animal development. *Development*. 138:1877–1892. http://dx.doi.org/10.1242/dev.054080

Guirao, B., A. Meunier, S. Mortaud, A. Aguilar, J.M. Corsi, L. Strehl, Y. Hirota, A. Desoeuvre, C. Boutin, Y.G. Han, et al. 2010. Coupling between hydrodynamic forces and planar cell polarity orients mammalian motile cilia. *Nat. Cell Biol.* 12:341–350. http://dx.doi.org/10.1038/ncb2040

Hashimoto, M., K. Shinohara, J. Wang, S. Ikeuchi, S. Yoshiba, C. Meno, S. Nonaka, S. Takada, K. Hatta, A. Wynshaw-Boris, and H. Hamada. 2010. Planar polarization of node cells determines the rotational axis of node cilia. *Nat. Cell Biol.* 12:170–176. http://dx.doi.org/10.1038/ncb2020

Huang, P., and A.F. Schier. 2009. Dampened Hedgehog signaling but normal Wnt signaling in zebrafish without cilia. *Development*. 136:3089–3098. http://dx.doi.org/10.1242/dev.041343

Ishida-Takagishi, M., A. Enomoto, N. Asai, K. Ushida, T. Watanabe, T. Hashimoto, T. Kato, L. Weng, S. Matsumoto, M. Asai, et al. 2012. The Dishevelled-associating protein Daple controls the non-canonical Wnt/Rac pathway and cell motility. *Nat Commun*. 3:859. http://dx.doi.org/10.1038/ncomms1861

Itoh, K., A. Jenny, M. Mlodzik, and S.Y. Sokol. 2009. Centrosomal localization of Diversin and its relevance to Wnt signaling. *J. Cell Sci.* 122:3791–3798. http://dx.doi.org/10.1242/jcs.057067

Jessen, J.R., J. Topczewski, S. Bingham, D.S. Sepich, F. Marlow, A. Chandrasekhar, and L. Solnica-Krezel. 2002. Zebrafish trilobite identifies new roles for Strabismus in gastrulation and neuronal movements. *Nat. Cell Biol.* 4:610–615.

Jones, C., and P. Chen. 2008. Primary cilia in planar cell polarity regulation of the inner ear. *Curr. Top. Dev. Biol.* 85:197–224. http://dx.doi.org/10.1016/S0070-2153(08)00808-9

Jones, C., V.C. Roper, I. Foucher, D. Qian, B. Banizs, C. Petit, B.K. Yoder, and P. Chen. 2008. Ciliary proteins link basal body polarization to planar cell polarity regulation. *Nat. Genet.* 40:69–77. http://dx.doi.org/10.1038/ng.2007.54

Karner, C.M., R. Chirumamilla, S. Aoki, P. Igarashi, J.B. Wallingford, and T.J. Carroll. 2009. Wnt9b signaling regulates planar cell polarity and kidney tubule morphogenesis. *Nat. Genet.* 41:793–799. http://dx.doi.org/10.1038/ng.400

Khanna, H., E.E. Davis, C.A. Murga-Zamalloa, A. Estrada-Cuzcano, I. Lopez, A.I. den Hollander, M.N. Zonneveld, M.I. Othman, N. Waseem, C.F. Chakarova, et al. 2009. A common allele in RPGRIP1L is a modifier of retinal degeneration in ciliopathies. *Nat. Genet.* 41:739–745. http://dx.doi.org/10.1038/ng.366

Kimmel, C.B., W.W. Ballard, S.R. Kimmel, B. Ullmann, and T.F. Schilling. 1995. Stages of embryonic development of the zebrafish. *Dev. Dyn.* 203:253–310. http://dx.doi.org/10.1002/aja.1002030302

Lancaster, M.A., J. Schroth, and J.G. Gleeson. 2011. Subcellular spatial regulation of canonical Wnt signalling at the primary cilium. *Nat. Cell Biol.* 13:700–707.

Link, V., A. Shevchenko, and C.P. Heisenberg. 2006. Proteomics of early zebrafish embryos. *BMC Dev. Biol.* 6:1. http://dx.doi.org/10.1186/1471-213X-6-1

May-Simera, H.L., A. Ross, S. Rix, A. Forge, P.L. Beales, and D.J. Jagger. 2009. Patterns of expression of Bardet-Biedl syndrome proteins in the mammalian cochlea suggest noncentrosomal functions. *J. Comp. Neurol.* 514:174–188. http://dx.doi.org/10.1002/cne.22001

Megason, S.G. 2009. In toto imaging of embryogenesis with confocal time-lapse microscopy. *Methods Mol. Biol.* 546:317–332. http://dx.doi.org/10.1007/978-1-60327-977-2_19

Megason, S.G., and S.E. Fraser. 2003. Digitizing life at the level of the cell: high-performance laser-scanning microscopy and image analysis for in toto imaging of development. *Mech. Dev.* 120:1407–1420. http://dx.doi.org/10.1016/j.mod.2003.07.005

Mitchell, B., J.L. Stubbs, F. Huisman, P. Taborek, C. Yu, and C. Kintner. 2009. The PCP pathway instructs the planar orientation of ciliated cells in the *Xenopus* larval skin. *Curr. Biol.* 19:924–929. http://dx.doi.org/10.1016/j.cub.2009.04.018

Montcouquiol, M., R.A. Rachel, P.J. Lanford, N.G. Copeland, N.A. Jenkins, and M.W. Kelley. 2003. Identification of Vangl2 and Scrb1 as planar polarity genes in mammals. *Nature*. 423:173–177. http://dx.doi.org/10.1038/nature01618

Montcouquiol, M., N. Sans, D. Huss, J. Kach, J.D. Dickman, A. Forge, R.A. Rachel, N.G. Copeland, N.A. Jenkins, D. Bogani, et al. 2006. Asymmetric localization of Vangl2 and Fz3 indicate novel mechanisms for planar cell polarity in mammals. *J. Neurosci.* 26:5265–5275. http://dx.doi.org/10.1523/JNEUROSCI.4680-05.2006

Montcouquiol, M., J.M. Jones, and N. Sans. 2008. Detection of planar polarity proteins in mammalian cochlea. *Methods Mol. Biol.* 468:207–219. http://dx.doi.org/10.1007/978-1-59745-249-6_16

Morgan, D., L. Eley, J. Sayer, T. Strachan, L.M. Yates, A.S. Craighead, and J.A. Goodship. 2002. Expression analyses and interaction with the anaphase promoting complex protein Apc2 suggest a role for inversin in primary cilia and involvement in the cell cycle. *Hum. Mol. Genet.* 11:3345–3350. http://dx.doi.org/10.1093/hmg/11.26.3345

Narimatsu, M., R. Bose, M. Pye, L. Zhang, B. Miller, P. Ching, R. Sakuma, V. Luga, L. Roncari, L. Attisano, and J.L. Wrana. 2009. Regulation of planar cell polarity by Smurf ubiquitin ligases. *Cell*. 137:295–307. http://dx.doi.org/10.1016/j.cell.2009.02.025

Otto, E.A., B. Schermer, T. Obara, J.F. O'Toole, K.S. Hiller, A.M. Mueller, R.G. Ruf, J. Hoefele, F. Beekmann, D. Landau, et al. 2003. Mutations in INVS encoding inversin cause nephronophthisis type 2, linking renal cystic disease to the function of primary cilia and left-right axis determination. *Nat . Genet.* 34:413–420. http://dx.doi.org/10.1038/ng1217

Park, T.J., B.J. Mitchell, P.B. Abitua, C. Kintner, and J.B. Wallingford. 2008. Dishevelled controls apical docking and planar polarization of basal bodies in ciliated epithelial cells. *Nat. Genet.* 40:871–879. http://dx.doi.org/10.1038/ng.104

Roepman, R., S.J. Letteboer, H.H. Arts, S.E. van Beersum, X. Lu, E. Krieger, P.A. Ferreira, and F.P. Cremers. 2005. Interaction of nephrocystin-4 and RPGRIP1 is disrupted by nephronophthisis or Leber congenital amaurosis-associated mutations. *Proc. Natl. Acad. Sci. USA*. 102:18520–18525. http://dx.doi.org/10.1073/pnas.0505774102

Ross, A.J., H. May-Simera, E.R. Eichers, M. Kai, J. Hill, D.J. Jagger, C.C. Leitch, J.P. Chapple, P.M. Munro, S. Fisher, et al. 2005. Disruption of Bardet-Biedl syndrome ciliary proteins perturbs planar cell polarity in vertebrates. *Nat. Genet.* 37:1135–1140. http://dx.doi.org/10.1038/ng1644

Roszko, I., A. Sawada, and L. Solnica-Krezel. 2009. Regulation of convergence and extension movements during vertebrate gastrulation by the Wnt/PCP pathway. *Semin. Cell Dev. Biol.* 20:986–997. http://dx.doi.org/10.1016/j.semcdb.2009.09.004

Sang, L., J.J. Miller, K.C. Corbit, R.H. Giles, M.J. Brauer, E.A. Otto, L.M. Baye, X. Wen, S.J. Scales, M. Kwong, et al. 2011. Mapping the NPHP-JBTS-MKS protein network reveals ciliopathy disease genes and pathways. *Cell*. 145:513–528. http://dx.doi.org/10.1016/j.cell.2011.04.019

Sayer, J.A., E.A. Otto, J.F. O'Toole, G. Nurnberg, M.A. Kennedy, C. Becker, H.C. Hennies, J. Helou, M. Attanasio, B.V. Fausett, et al. 2006. The centrosomal protein nephrocystin-6 is mutated in Joubert syndrome and activates transcription factor ATF4. *Nat. Genet.* 38:674–681. http://dx.doi.org/10.1038/ng1786

Schwarz-Romond, T., C. Merrifield, B.J. Nichols, and M. Bienz. 2005. The Wnt signalling effector Dishevelled forms dynamic protein assemblies rather than stable associations with cytoplasmic vesicles. *J. Cell Sci.* 118:5269–5277. http://dx.doi.org/10.1242/jcs.02646

Ségalen, M., C.A. Johnston, C.A. Martin, J.G. Dumortier, K.E. Prehoda, N.B. David, C.Q. Doe, and Y. Bellaïche. 2010. The Fz-Dsh planar cell polarity pathway induces oriented cell division via Mud/NuMA in *Drosophila* and zebrafish. *Dev. Cell*. 19:740–752. http://dx.doi.org/10.1016/j.devcel.2010.10.004

Sepich, D.S., M. Usmani, S. Pawlicki, and L. Solnica-Krezel. 2011. Wnt/PCP signaling controls intracellular position of MTOCs during gastrulation convergence and extension movements. *Development*. 138:543–552. http://dx.doi.org/10.1242/dev.053959

Sharma, N., N.F. Berbari, and B.K. Yoder. 2008. Ciliary dysfunction in developmental abnormalities and diseases. *Curr. Top. Dev. Biol.* 85:371–427. http://dx.doi.org/10.1016/S0070-2153(08)00813-2

Simons, M., J. Gloy, A. Ganner, A. Bullerkotte, M. Bashkurov, C. Krönig, B. Schermer, T. Benzing, O.A. Cabello, A. Jenny, et al. 2005. Inversin, the gene product mutated in nephronophthisis type II, functions as a

molecular switch between Wnt signaling pathways. *Nat. Genet.* 37:537–543. http://dx.doi.org/10.1038/ng1552

Sipe, C.W., and X. Lu. 2011. Kif3a regulates planar polarization of auditory hair cells through both ciliary and non-ciliary mechanisms. *Development*. 138:3441–3449. http://dx.doi.org/10.1242/dev.065961

Smith, W.C., and R.M. Harland. 1991. Injected Xwnt-8 RNA acts early in *Xenopus* embryos to promote formation of a vegetal dorsalizing center. *Cell*. 67:753–765. http://dx.doi.org/10.1016/0092-8674(91)90070-F

Song, H., J. Hu, W. Chen, G. Elliott, P. Andre, B. Gao, and Y. Yang. 2010. Planar cell polarity breaks bilateral symmetry by controlling ciliary positioning. *Nature*. 466:378–382. http://dx.doi.org/10.1038/nature09129

Vierkotten, J., R. Dildrop, T. Peters, B. Wang, and U. Rüther. 2007. Ftm is a novel basal body protein of cilia involved in Shh signalling. *Development*. 134:2569–2577. http://dx.doi.org/10.1242/dev.003715

Wallingford, J.B. 2010. Planar cell polarity signaling, cilia and polarized ciliary beating. *Curr. Opin. Cell Biol.* 22:597–604. http://dx.doi.org/10.1016/j.ceb.2010.07.011

Wallingford, J.B., and B. Mitchell. 2011. Strange as it may seem: the many links between Wnt signaling, planar cell polarity, and cilia. *Genes Dev.* 25:201–213. http://dx.doi.org/10.1101/gad.2008011

Wang, J., S. Mark, X. Zhang, D. Qian, S.J. Yoo, K. Radde-Gallwitz, Y. Zhang, X. Lin, A. Collazo, A. Wynshaw-Boris, and P. Chen. 2005. Regulation of polarized extension and planar cell polarity in the cochlea by the vertebrate PCP pathway. *Nat. Genet.* 37:980–985. http://dx.doi.org/10.1038/ng1622

Wang, J., N.S. Hamblet, S. Mark, M.E. Dickinson, B.C. Brinkman, N. Segil, S.E. Fraser, P. Chen, J.B. Wallingford, and A. Wynshaw-Boris. 2006. Dishevelled genes mediate a conserved mammalian PCP pathway to regulate convergent extension during neurulation. *Development*. 133:1767–1778. http://dx.doi.org/10.1242/dev.02347

Williams, C.L., C. Li, K. Kida, P.N. Inglis, S. Mohan, L. Semenec, N.J. Bialas, R.M. Stupay, N. Chen, O.E. Blacque, et al. 2011. MKS and NPHP modules cooperate to establish basal body/transition zone membrane associations and ciliary gate function during ciliogenesis. *J. Cell Biol.* 192:1023–1041. http://dx.doi.org/10.1083/jcb.201012116

Zaghloul, N.A., and N. Katsanis. 2010. Functional modules, mutational load and human genetic disease. *Trends Genet.* 26:168–176. http://dx.doi.org/10.1016/j.tig.2010.01.006

Zhao, C., and J. Malicki. 2011. Nephrocystins and MKS proteins interact with IFT particle and facilitate transport of selected ciliary cargos. *EMBO J.* 30:2532–2544. http://dx.doi.org/10.1038/emboj.2011.165

Zufferey, R., T. Dull, R.J. Mandel, A. Bukovsky, D. Quiroz, L. Naldini, and D. Trono. 1998. Self-inactivating lentivirus vector for safe and efficient in vivo gene delivery. *J. Virol.* 72:9873–9880.